**NASA TECHNICAL NOTE**

NASA TN D-6221

# CALCULATION BY A FINITE-DIFFERENCE METHOD OF SUPERSONIC TURBULENT BOUNDARY LAYERS WITH TANGENTIAL SLOT INJECTION

*by Ivan E. Beckwith and Dennis M. Bushnell*

*Langley Research Center*
*Hampton, Va. 23365*

NATIONAL AERONAUTICS AND SPACE ADMINISTRATION • WASHINGTON, D. C. • APRIL 1971

| 1. Report No.<br>NASA TN D-6221 | 2. Government Accession No. | 3. Recipient's Catalog No. |
|---|---|---|
| 4. Title and Subtitle<br>CALCULATION BY A FINITE-DIFFERENCE METHOD OF SUPERSONIC TURBULENT BOUNDARY LAYERS WITH TANGENTIAL SLOT INJECTION | | 5. Report Date<br>April 1971 |
| | | 6. Performing Organization Code |
| 7. Author(s)<br>Ivan E. Beckwith and Dennis M. Bushnell | | 8. Performing Organization Report No.<br>L-7515 |
| 9. Performing Organization Name and Address<br>NASA Langley Research Center<br>Hampton, Va. 23365 | | 10. Work Unit No.<br>129-01-20-09 |
| | | 11. Contract or Grant No. |
| 12. Sponsoring Agency Name and Address<br>National Aeronautics and Space Administration<br>Washington, D.C. 20546 | | 13. Type of Report and Period Covered<br>Technical Note |
| | | 14. Sponsoring Agency Code |

15. Supplementary Notes

With appendix by Barbara A. Hixon and Dennis M. Bushnell

16. Abstract

A method based on eddy-diffusivity and mixing-length concepts has been developed for calculating turbulent boundary layers with tangential slot injection. The partial differential equations for the mean motion are solved by a finite-difference procedure. Comparisons of predicted velocity profiles, boundary-layer thicknesses, heat transfer, skin friction, and recovery temperatures have been made with experimental data from previous investigations at free-stream Mach numbers of 3 and 6. Prediction and experiment showed good agreement over the range of conditions and locations available, including just downstream of the slot where maximum reductions in skin friction occurred. Details of the mixing-length relations and computer program are included.

| 17. Key Words (Suggested by Author(s))<br>Finite-difference method<br>Turbulent boundary layer<br>Tangential slot injection | 18. Distribution Statement<br>Unclassified — Unlimited | | |
|---|---|---|---|
| 19. Security Classif. (of this report)<br>Unclassified | 20. Security Classif. (of this page)<br>Unclassified | 21. No. of Pages<br>74 | 22. Price*<br>$3.00 |

*For sale by the National Technical Information Service, Springfield, Virginia 22151

# CALCULATION BY A FINITE-DIFFERENCE METHOD OF
# SUPERSONIC TURBULENT BOUNDARY LAYERS
# WITH TANGENTIAL SLOT INJECTION

By Ivan E. Beckwith and Dennis M. Bushnell
Langley Research Center

## SUMMARY

A method has been developed for calculating compressible turbulent boundary layers with tangential slot injection of homogeneous gas species. The partial differential equations for the mean motion are solved by an implicit finite-difference method. The turbulent-flux terms are modeled by means of eddy-diffusivity and mixing-length concepts. The magnitude and distribution of the mixing length across the boundary layer are determined from the computed characteristics of the free-mixing region between the injected jet and the initial boundary layer. The development of this mixing region and its interaction with the wall and external boundary layer are calculated from the species-conservation equation which, in the present computer program, is used to calculate the behavior of a trace species.

The method is described in detail, and the appropriate initial and boundary conditions used to calculate the concentration of the trace species and the corresponding mixing-length relations are also described. The numerical-solution procedure is similar to that contained in a previous computer program developed at NASA Langley Research Center to solve conventional boundary-layer problems. The modifications to the previous program required to solve the present slot-injection problem are described and listed in FORTRAN IV in the appendix of this report.

Comparisons of predicted velocity profiles, boundary-layer thicknesses, heat transfer, skin friction, and recovery temperatures (or effectiveness) have been made with results from four previous experimental investigations at free-stream Mach numbers of 3 and 6. Agreement with experimental data was generally good. In particular, good predictions were obtained of velocity profiles and surface properties in the region just downstream of the slot where no previous method has been successful even for low-speed flows. The generally good agreement obtained between theoretical results and experimental data indicates that reliable predictions can be obtained for slot-injection flows by the present method even when the inherent restriction of small normal pressure gradients in boundary-layer theory is violated.

# INTRODUCTION

Injection from slots into turbulent boundary layers has long been advocated as a method of controlling the downstream-wall temperature and skin friction. The injection of heated air is a well-known and effective deicing method. (See ref. 1.) In hot environments, the injection of cool air from either a slot or porous strip is usually referred to as film cooling since it provides thermal protection for the downstream surface. (See refs. 2 and 3, for example.) When the injected fluid is directed downstream through a rearward-facing tangential slot, the skin friction generally increases or decreases according to whether the specific momentum of the jet is greater than or less than that of the free stream. With jet momentum greater than free-stream momentum, the flow configuration is often referred to as a wall jet, and the resulting increase in skin friction may be utilized to delay separation. A recent review of experimental data and integral theories for such flows is given in reference 4. The cooling effects of wall jets have been investigated for incompressible flow in reference 5 where it was shown that Colburn's Reynolds analogy, expressed in terms of the maximum velocity in the wall jet and applied to empirical correlations of skin-friction data, gave satisfactory predictions of the measured heating for this type of flow in the region far downstream of the slot.

The flows to be considered in the present report will be primarily those where the momentum of the tangentially injected fluid is less than that of the free stream, and some reduction in skin friction might be expected. Because of the possibility of simultaneous thermal protection and skin-friction reduction, there is continuing interest in this type of film cooling and, consequently, a large amount of literature is available on the subject.

Typical experimental results and correlations of film cooling effectiveness for incompressible flows with constant free-stream velocities are given in references 1 and 6 to 9. Comparisons in reference 8 of data from some of these investigations and the subsonic compressible data of reference 2 indicated the effectiveness (a normalized form of the local adiabatic-wall temperature) may vary considerably with changes in slot configuration, ratios of slot height to initial boundary-layer thickness, mass-injection ratios, and compressibility effects. These comparisons have led to several investigations (refs. 10 to 13) concerned with various aspects of slot geometry, such as slot width or height, injection angle, and lip thickness. In practical applications of film cooling, several other effects must also be considered, such as those caused by foreign-gas injection, variable free-stream velocities, and multiple slots.

The influence of foreign-gas injection, which may introduce large density variations even in low-speed flow, has been investigated in references 13 and 14. The effects of variable free-stream velocity have been reported in references 15 and 16, where it is indicated that film cooling effectiveness is reduced by strong accelerations downstream

of the slot. Experimental data and approximate methods for computing wall temperature downstream of multiple slots are presented in references 17 to 20.

Most of the references for slot injection discussed thus far are for low-speed flows, where compressibility effects due to high velocities are negligible. Experimental data for higher speeds but subsonic free-stream Mach numbers are reported in references 2 and 16. In reference 20, injection into supersonic turbulent boundary layers has been treated by reference-enthalpy methods applied to correlations of low-speed data. Experimental data and correlations or approximate theoretical analyses for tangential slot injection into supersonic turbulent flows are also available in references 21 to 29. Detailed boundary-layer-profile data for these conditions are available only in references 21 to 23.

Velocity-profile data for injection from a sonic slot into a flat-plate turbulent boundary layer at a free-stream Mach number of 3.0 are given in reference 21. The main purpose of this investigation was to measure skin friction and drag, and no data were obtained on film cooling effectiveness since the total temperatures of the slot and free-stream flow were nearly equal ($294^O$ K ($530^O$ R) and $317^O$ K ($570^O$ R), respectively).

The investigations of references 22 to 24 were at a free-stream Mach number of 6.0 with free-stream and slot-flow total temperatures of about $444^O$ K ($800^O$ R) and $294^O$ K ($530^O$ R), respectively. However, adiabatic temperatures were not measured directly in any of these investigations; instead, the film cooling effectiveness was inferred from measured heating rates and calculated heat-transfer coefficients from the flat-plate reference-enthalpy method of Eckert (ref. 30). Comparisons in reference 22 of these results at Mach 6 with previous data indicated that film cooling may be much more effective in hypersonic flow than in subsonic flow. However, the indirect procedure for calculating adiabatic-wall temperatures, as used in references 22 to 24, is questionable because the calculated heat-transfer coefficients based on flat-plate equilibrium flow do not apply to slot-injection flows. The actual values of heat-transfer coefficients in a boundary layer perturbed by rapid changes in surface temperature (such as occurs with slot injection) are known to deviate considerably from the values for an undisturbed boundary layer as shown, for example, by the results of reference 31 and by the analysis of reference 32. The analysis of reference 32 was used to predict the adiabatic-wall-temperature distribution for the experimental investigation of reference 1 by means of a specified step function in surface heat transfer. This step function simulated the heat addition at the slot. While the predicted values of effectiveness were about 20 percent too high, the predicted trend with downstream distance and mass-injection ratio was the same as that of the data in the far-slot region. Hence, the dominant factor that determines the adiabatic-wall temperature in the far-slot region for low-speed flows is the initial energy content of the flow near the wall. However, in the near-slot region the momentum transfer

between the jet and initial boundary layer is probably of crucial importance. In particular, Colburn's Reynolds analogy factor may not be applicable in this region because of the different structure and rapid changes in the velocity and thermal mixing layers. Also, when the injected momentum is less than the free-stream value, in contrast with the wall jet (ref. 5), there is no consistent reference velocity close to the wall that can be used to formulate a simple Reynolds analogy expression.

Adiabatic-wall temperatures downstream of an injection slot were measured directly for the first time in hypersonic flow in the investigation of reference 29 which was also at a free-stream Mach number of 6.0. These results indicated that significant improvements over subsonic and low Mach number supersonic results can be expected in both the extent of the thermal protection and in the relaxation rate to undisturbed equilibrium temperatures.

It is not known whether these increased efficiencies of slot cooling observed in references 22 and 29 are due to slower mixing rates in the hypersonic boundary layers or to the relatively small ratios of slot height to initial boundary-layer thickness (0.01 to 0.2) used in these investigations. One approach to such problems is by means of finite-difference solutions of the flow field with the complete initial and boundary conditions included. At the present time, solution techniques for the complete equations of motion, including the normal momentum equation (see ref. 33, for example), are impractical for engineering applications because of the lengthy relaxation procedure and large number of mesh points required to obtain good accuracy within an entire flow field for which all boundary conditions must be specified. Furthermore, the results would be only as good as the models of the turbulent-flux terms.

When the normal pressure gradients can be neglected, the general equations reduce to the conventional boundary-layer equations, which are parabolic and hence can be solved by forward-marching techniques with only the initial conditions and boundary conditions in the free stream and at the wall required. Models for the turbulent-flux terms can then be developed and tested with these simpler flows and computing procedures. Both explicit (ref. 34) and implicit methods (refs. 35 to 37) have been applied successfully to turbulent-boundary-layer flows without slot injection.

The method of reference 37 has also been used extensively to calculate low-speed turbulent-boundary-layer flows with tangential slot injection. (See refs. 14 and 38, for example.) A simple two-step ramp function for the Prandtl mixing length was used in these calculations, and good predictions were obtained for profiles and film cooling effectiveness except in regions less than 20 slot heights downstream of the slot. Experimental data for low-speed flows (ref. 39) show that normal pressure gradients are small for downstream distances from the slot of greater than 20 slot heights when the ratios of injection velocity to free-stream velocity are less than unity.

4

For slot injection into supersonic flow, however, large disturbances which propagate far downstream are generated at the slot (refs. 25 and 27) unless the slot static pressure is carefully matched to the local-stream static pressure, as in reference 26. As pointed out in reference 27, the flow field that results when large differences in slot and stream static pressure are present cannot be computed with the conventional boundary-layer equations. The shock and expansion waves that dominate the flow for this "mismatched" pressure condition can only be accurately accounted for by the complete equations of motion.

The purpose of the present investigation is to determine if the characteristics of supersonic turbulent boundary layers with tangential slot injection can be predicted with the finite-difference method of reference 36. Since the normal-momentum equation is neglected, the results may not apply when the static pressure at the slot exit differs from the local-stream static pressure, or when the slot-injection flow is inclined at an appreciable angle to the local-flow direction. In an attempt to improve predictions in the important region just downstream of the slot, the simple-ramp mixing-length distribution, as used in references 14, 37, and 38, has been modified to account for the rapidly changing flow structure in this region. Again, the results may be questionable when the slot-lip thickness is appreciable compared with the slot height since for incompressible flow the effects of the thick lip influence the flow far downstream to distances of 100 or more slot heights. (See refs. 12 and 13.) The present theoretical predictions will be compared with the experimental data of references 21 to 24 and 29 for free-stream Mach numbers of 3.0 and 6.0. While the present method has not yet been applied extensively to subsonic or incompressible slot-injection flows, preliminary results for such flows (not reported herein) indicate that reliable predictions can be obtained. For the present applications, it should be noted that in the investigations of references 21 to 24 and 29, the restrictions mentioned previously regarding matched static pressures, small injection angles, and lip thickness were generally violated to some extent.

Modifications to the original boundary-layer computer program (ref. 41) required to compute the present slot-injection flows are given in the appendix by Barbara A. Hixon and Dennis M. Bushnell.

## SYMBOLS

Measurements and calculations were made in the U.S. Customary Units. They are presented herein in the International System of Units (SI) with the equivalent values given parenthetically in the U.S. Customary Units.

$A$        Van Driest's damping parameter, $\dfrac{A_d \mu}{\rho \sqrt{\tau_w / \rho}}$   (see eq. (3))

$A_d$      damping constant, 26 for zero mass transfer by normal injection at wall

$a$      ratio of mixing length to width of various flow regions (see eqs. (14) and (18))

$C_f$      skin-friction coefficient, $\dfrac{2\tau_w}{\rho_e u_e^2}$

$C_i$      mass concentration of species i, $\dfrac{\rho_i}{\rho}$

$c_p$      specific heat at constant pressure

$D$      diffusion coefficient of species i

$F$      velocity-profile variable, $\dfrac{\bar{u}}{u_e}$

$f$      mixing-length function from reference 36 (see eqs. (4))

$G$      normalized concentration profile, $\dfrac{\overline{C}_i - C_{i,w}}{C_{i,e} - C_{i,w}}$

$g$      ratio of local to edge concentration of species i, $\dfrac{\overline{C}_i}{C_{i,e}}$

$H$      total enthalpy, $h + \dfrac{u^2}{2}$

$H_{in}^* = \dfrac{\delta_{in}^*}{\theta_{in}}$

$h$      static enthalpy

$K$      constant in Prandtl's mixing-length relation, taken as 0.4 herein (see eq. (4a))

$L$      reference length

$l$      mixing length

$M$      Mach number

6

m       molecular weight

$N_{Le}$       Lewis number

$N_{Pr}$       Prandtl number

$N_{Re}$       Reynolds number, $\dfrac{\rho_e u_e x}{\mu_e}$

$N_{Sc}$       Schmidt number

$N_{St}$       Stanton number

p       pressure

$\dot{q}$       heat-transfer rate

R       universal gas constant

r       radius from axis of symmetry

s       slot height (see fig. 1)

T       absolute temperature

t       thickness of slot lip (see fig. 1)

u,v       velocity components in x,y directions

$\tilde{v} = \bar{v} + \dfrac{\overline{\rho' v'}}{\bar{\rho}}$

W       height of concentration mixing region

X       correlating parameter for streamwise distance and mass flow, $\dfrac{\Delta x}{s}(\lambda)^{-0.8}$

x,y       boundary-layer coordinates, parallel (in flow direction) and normal to surface. For free turbulent flows, y is distance from plane of symmetry for jets and distance from plane where $u = \frac{1}{2}\left(\bar{u}_{max} + \bar{u}_{min}\right)$ for half jets.

7

$\Delta x = x - x_0$

$\gamma$          ratio of specific heats

$\delta$          boundary-layer thickness evaluated where $F = 0.995$ unless otherwise noted

$\delta_r$          initial total flow thickness, $\delta_0 + t + s$

$\delta_{in}^* = \int_0^\delta (1 - F)dy$      $\left(\text{For the present problem, the lower limit is replaced by } y \text{ at } G = 0.01 \text{ to give } \delta_{in,s}^*\right)$

$\epsilon$          eddy viscosity (see eq. (1))

$\zeta$          ratio of local stagnation temperature to free-stream stagnation temperature, $\overline{T}_t / T_{t,e}$

$\eta$          recovery-temperature effectiveness, $\dfrac{T_{t,e} - T_{aw}}{T_{t,e} - \overline{\overline{T}}_{t,j,o}}$

$\overline{\Theta}$          total enthalpy variable, $\dfrac{\overline{H} - H_w}{H_e - H_w}$

$\theta = \int_0^\delta \dfrac{\overline{\rho}F}{\rho_e}(1 - F)dy$

$\theta_{in} = \int_0^\delta F(1 - F)dy$      $\left(\text{For the present problem, the lower limit is replaced by } y \text{ at } G = 0.01 \text{ to give } \theta_{in,s}\right)$

$\kappa$          mixing-length factor for pipe or channel flows

$\lambda$          specific mass-flow ratio of injected flow to free-stream flow, $\left(\dfrac{1}{s}\int_0^s \dfrac{\overline{\rho}}{\rho_e} F \, dy\right)_{x_0}$

$\mu$          molecular viscosity

$\rho$          density

8

| $\tau$ | shear stress |
|--------|--------------|
| $\omega$ | recovery factor (see eq. (32)) |

Subscripts:

| A | air |
|---|-----|
| av | average or mean |
| aw | adiabatic wall |
| b | outer part of boundary-layer region with slot injection |
| c | concentration |
| e | "edge" of boundary layer where specified boundary-layer profile parameters $F$, $\overline{\Theta}$, or $g \rightarrow 0.9999$ |
| f | far-wall region of boundary layer |
| i | species |
| j | jet region |
| m | free turbulent mixing region |
| max | maximum |
| min | minimum |
| n | near-wall region of boundary layer |
| o | initial values or station, usually at slot exit |
| r | reference |
| s | slot injection flow |

T          turbulent

t          local stagnation conditions

u          velocity

w          wall

0.5        point in a jet flow where the velocity is $\frac{1}{2}\left(\bar{u}_{max} + \bar{u}_{min}\right)$ or concentration is $\frac{1}{2}\left(\overline{C}_{i,max} + \overline{C}_{i,min}\right)$

A bar over a symbol denotes a time mean value, and a prime denotes a fluctuating value.

A double prime denotes evaluation at the reference temperature given by equation (33).

## THEORY

The method used in the present investigation to solve the boundary-layer equations for compressible turbulent flow is similar to that used by the authors in previous work reported in references 36 and 40. An implicit finite-difference method is used to solve the nonlinear partial differential equations for the conservation of mass, momentum, and total enthalpy for the mean flow. Details of the numerical procedure and the computer program for conventional boundary-layer flows are available in reference 41. The modifications to the previous computer program required to solve the present problem are described and listed in FORTRAN IV in the appendix.

In this section, the eddy-viscosity and mixing-length expressions developed previously by the authors for calculating turbulent boundary layers without slot injection will first be reviewed briefly. The extensions and modifications of these expressions to calculate the rapidly changing profiles of velocity, temperature, and concentration just downstream of the slot and in the subsequent relaxation region (where the profiles relax to those for an undisturbed boundary layer far downstream of the slot) will then be described. In accordance with previous results for compressible turbulent boundary layers (refs. 34 to 36, 40, and 42, for example), kinematic scales are used in the eddy-viscosity and mixing-length models. Mixing-length relations determined from incompressible flows are then applied directly to the present problem.

10

## Turbulent Flux of Momentum and Enthalpy

The turbulent-flux terms in the boundary-layer equations are modeled by eddy-viscosity and turbulent Prandtl number concepts, where

$$\tau_T = \epsilon \frac{\partial \bar{u}}{\partial y} \quad \text{and} \quad \dot{q}_T = \frac{\epsilon}{N_{Pr,T}} \frac{\partial \bar{h}}{\partial y} \tag{1}$$

For the boundary-layer flows treated previously (refs. 36 and 40), the eddy viscosity was formulated according to Prandtl's mixing-length relation

$$\epsilon = \bar{\rho} \ell_u^2 \left| \frac{\partial \bar{u}}{\partial y} \right| \tag{2}$$

where generally

$$\frac{\ell_u}{\delta} = \left[ 1 - \exp\left(\frac{-y}{A}\right) \right] f\left(x, \frac{y}{\delta}\right) \tag{3}$$

The quantity within the brackets of equation (3) is Van Driest's damping function, which has been modified (ref. 36) to account for the effects of mass transfer on the viscous sub-layer. For conventional boundary layers, the function $f(x, y/\delta)$ consists of two parts. These two parts apply, respectively, to the near-wall and far-wall regions, where the function was assumed to be (ref. 36)

$$f_n = K \frac{y}{\delta} \qquad \qquad \left( \frac{y}{\delta} \leq 0.1 \right) \tag{4a}$$

$$f_f = \left( \frac{\ell}{\delta} \right)_f = f_f\left( H_{in}^* \right) \qquad \qquad \left( \frac{y}{\delta} \geq 0.3 \right) \tag{4b}$$

where the form for $f_f$ used herein is

$$f_f = 0.265 - 0.196 H_{in}^* + 0.0438 H_{in}^{*2} \tag{4c}$$

Equation (4a) is Prandtl's wall function, which seems to be universally applicable. Equation (4c) accounts partially for the effects of pressure gradient on the outer, or wake, portion of a boundary layer. The limiting values of $f_n$ and $f_f$ at $\frac{y}{\delta} = 0.1$ and 0.3 are connected by a straight-line segment. In the present calculations, $K = 0.4$ has been used throughout.

The basic concept of eddy viscosity, as expressed by equations (1), is known to be faulty (see ref. 43, for example), particularly when the velocity profiles have maximum

or minimum values within the boundary layer, as in slot-injection flows. For these flows, equations (1) require that when $\frac{\partial \bar{u}}{\partial y} = 0$, then $\tau_T = 0$. This condition is not in agreement with experimental observations. An analysis in reference 43 of several sets of experimental data, including a wall-jet flow, has indicated that the addition of another term proportional to the product,

$$\left( \frac{\partial}{\partial y} \sqrt{\overline{v'^2}} \right) \frac{\partial^2 \bar{u}}{\partial y^2}$$

would impart the correct behavior to the expression for turbulent shear. This additional term is not used herein because its effect is generally small and also because values of $\overline{v'^2}$, which are not generally available, would be required.

Considerable success has already been achieved (refs. 14, 37, and 38) in the calculation of turbulent boundary layers with slot injection for $\frac{\Delta x}{s} > 20$ by using simple eddy-viscosity and mixing-length relations similar to those of equations (1) to (4). However, for applications of interest herein, the initial relaxation region where $\frac{\Delta x}{s} < 20$ is critical, not only regarding predictions for the extent and magnitude of thermal protection, but particularly with respect to the validity of skin-friction predictions. In applications of slot cooling to hypersonic cruise aircraft, for example, the magnitude of reductions in skin friction may determine the overall feasibility of the slot-cooling system. The following models have therefore been developed primarily to provide improved predictions in this near-slot region.

### Modified Mixing-Length Expressions

The type of flow to be computed is illustrated by the schematic sketches of figure 1. Injection occurs at $x = x_0$ from a tangential slot of height $s$ with the velocity profiles specified in the slot and across the initial boundary layer of thickness $\delta_0$. If the slot-lip thickness $t$ is appreciable compared with the slot height $s$ (greater than about 0.1s), the profiles just downstream of the lip would be affected by local separation and reverse flow caused by the thick lip. Since the present method is based on the boundary-layer equations, the flow in the separated region cannot be computed accurately. Hence, the initial profiles used to start the calculation should be located downstream of any separated region. For the present purpose, this downstream distance can be taken as about 2t where the input velocity profiles would be specified, as indicated in figure 1(a). The initial boundary-layer flow mixes with the injected jet flow by turbulent diffusion or mixing processes. Far downstream, the velocity profiles tend to approach those of an undisturbed turbulent boundary layer. The corresponding development of concentration

profiles of air with foreign-gas injection at the slot is depicted in figure 1(b). Note that with this type of flow, the mixing region and concentration profiles could readily be measured by suitable experimental procedures. Presumably, the mixing process is completed when the concentration of air at the wall approaches the free-stream value.

In figure 1(c), possible mixing-length distributions are shown. Three general objectives of the present mixing-length expressions are (1) generally accepted distributions of mixing length would be used at the initial input station just downstream of the slot location; (2) this initial distribution would be modified in a reasonable and realistic manner to represent the early development and spread of the mixing region; and (3) the calculated relaxation of the jet and mixing regions of the flow to the undisturbed boundary layer far downstream would govern the corresponding mixing-length distributions. The mixing-length expressions developed to achieve these objectives and the resulting distributions of mixing length will be described in the following sections. In order to accurately define and "track" the mixing region downstream of the slot, the species-conservation equation is utilized.

In the present computer program, the foreign species is assumed to have the same molecular weight and viscosity as air. The present calculations for the concentration of a foreign species then represent the physical behavior of a trace species mixed with air.

Conservation of species.- For no chemical reactions, this equation is written for species $i$ as

$$\bar{\rho}\bar{u}\,\frac{\partial \bar{C}_i}{\partial x} + \bar{\rho}\tilde{v}\,\frac{\partial \bar{C}_i}{\partial y} = \frac{\partial}{\partial y}\left[\bar{\rho}D\,\frac{\partial \bar{C}_i}{\partial y} - \overline{(\rho v)'C_i'}\right] \tag{5}$$

A turbulent diffusion coefficient $D_T$ and a diffusion mixing length $l_c$ may be defined by the relations

$$-\overline{(\rho v)'C_i'} = \bar{\rho}D_T\,\frac{\partial \bar{C}_i}{\partial y} = \bar{\rho}l_u l_c\left|\frac{\partial \bar{u}}{\partial y}\right|\frac{\partial \bar{C}_i}{\partial y} \tag{6}$$

With the use of equation (2), the turbulent Schmidt number $N_{Sc,T}$ is then simply a ratio of momentum to diffusion mixing lengths

$$N_{Sc,T} = \frac{\epsilon}{\bar{\rho}D_T} = \frac{l_u}{l_c} \tag{7}$$

In terms of the concentration profile

$$g = \frac{\bar{C}_i}{C_{i,e}} \tag{8}$$

13

equation (5) can be written as $\left(\text{where }\; C_{i,e}\;\text{ is assumed constant}\right)$

$$\bar{\rho}\bar{u}\,\frac{\partial g}{\partial x} + \bar{\rho}\tilde{v}\,\frac{\partial g}{\partial y} = \frac{\partial}{\partial y}\left[\left(\frac{\mu}{N_{Sc}} + \frac{\epsilon}{N_{Sc,T}}\right)\frac{\partial g}{\partial y}\right] \tag{9}$$

The boundary conditions for $g$ used in the present solutions for $y = 0$ are

$$g = g_w \tag{10a}$$

or, for zero mass transfer at the surface

$$\left(\frac{\partial g}{\partial y}\right)_w = 0 \tag{10b}$$

At the outer edge of the concentration field, $\overline{C}_i \rightarrow C_{i,e}$; hence, for $y = y_e$

$$g = 1 \tag{10c}$$

The requirement of equation (10b) is based on the basic relation between diffusional velocity of species $i$ and the concentration gradient. Hence, for zero mass transfer at the surface, which is the only boundary condition considered herein, $\left(\dfrac{\partial \overline{C}_i}{\partial y}\right)_w = 0.$ The computation procedure for satisfying this boundary condition is described in the appendix.

Equation system.- Equation (9) is solved as part of the system of equations for the conservation of mass, momentum, and total enthalpy by the same implicit numerical method used in reference 36 and given in detail in reference 41. These latter equations will not be repeated here since they are identical to those shown in references 36 and 41 provided that the molecular and turbulent Lewis numbers are assumed to be unity. This assumption is used herein. For flows where the turbulent flux of momentum and energy is much larger than the corresponding molecular flux, the molecular-transfer terms can be neglected entirely except in the near-wall region. The assumption of unity for the turbulent Lewis number is based on the experimental data of reference 44, where the linear relation between $\overline{C}_i$ and $\overline{\Theta}$ showed that $N_{Le,T} \approx 1.0$ for air-air and hydrogen-air mixing of subsonic coaxial streams.

The computation procedure of references 36 and 41 must be changed, however, when the recovery temperature of the wall is required. The boundary condition at the wall $H_w(x)$ for a specified wall-temperature distribution is replaced by the condition

$$\left(\frac{\partial \overline{H}}{\partial y}\right)_w = 0 \tag{10d}$$

and the energy equation is solved directly in terms of $\zeta = \overline{H}/H_e$ rather than in terms of $\overline{\Theta}$. In this way, the values of $\zeta_{aw}$ are obtained directly from the numerical solutions. The procedure is the same as that used to satisfy the boundary condition (10b) and is described and listed in the appendix.

The equation of state to be used with the new system of equations would, in general, account for the mixing of different gases since the instantaneous properties of the gases are related by

$$p = \rho RT \sum_i \frac{c_i}{m_i} \tag{11}$$

When the injected and free-stream gases have the same molecular weight as in the present computer program,

$$m_i = m \tag{12}$$

The mean properties are then related by

$$\overline{p} = \frac{R}{m}\left(\overline{\rho}\overline{T} + \overline{\rho'T'}\right) \tag{13}$$

The correlation term $\overline{\rho'T'}$ has been neglected in all solutions on the basis of the results and discussion in reference 45, which indicates that for stream Mach numbers up to about 9, this term would decrease $\overline{p}$ by only a few percent.

Calculation of initial mixing region.- Since the system of equations to be solved is parabolic, initial conditions for all dependent variables are required. These initial values for velocity, concentration (illustrated in fig. 1), and enthalpy are specified as profile shapes or functions of $y$ at the initial station $x_0$. That is, the functions $F(x_0,y)$, $g(x_0,y)$, and $\overline{\Theta}(x_0,y)$ $\left(\text{or } \zeta(x_0,y) \text{ for boundary condition } 10(d)\right)$ must be specified. If possible, these initial profile shapes should be based on experimental data for the particular configuration of interest. In the absence of experimental data for the external flow just upstream of the slot and the flow within the slot at its exit, suitable approximations for these $F$ and $\overline{\Theta}$ profiles can usually be provided on the basis of general knowledge of two-dimensional (or axisymmetric) boundary-layer and channel flows. However, it is important to include any upstream "history" effects (that is, the effects of static pressure and wall-temperature gradients) in these initial profiles for $F$ and $\overline{\Theta}$. If these effects are thought to be significant, finite-difference solutions for the upstream flow should be used unless reliable experimental data are available.

With the present definition of  g  (eq. (8)), the initial concentration profile is supplied as essentially a step function, with  $g = 0$  at the slot exit and  $g = 1$  for the external flow.  Thus, for example, in a problem with foreign-gas injection from the slot into an air boundary layer, the concentration  $\overline{C}_i$  represents the concentration of air in the mixture of air and foreign gas.  (See fig. 1.)  The molecular weight (and density) of the mixture is then governed by the general equation of state (eq. (11)) according to the local values of  $\overline{C}_i$  determined from the solution of the complete system of equations.

When the injected and external gases are homogeneous, as in the present computer program, the initial profile for  g  would be the same as that with foreign-gas injection, but the conventional equation of state (eq. (13)) is used and the physical interpretation of  $\overline{C}_i$  then corresponds to the concentration of a "trace" species which can have no direct physical effect on the velocity and temperature field.  The "edges" of the mixing layer are then determined at any station from the computed values of  g  by specifying (in the present calculations) the inside edge nearest the wall as the value of  y  where  $G = 0.01$  and the outside edge as the value of  y  where  $G = 0.99$.  In the same way, the nominal center of the mixing region is specified as the value of  y  where  $G = 0.5$.  (See fig. 1(b).)

Mixing length in free turbulent mixing region.- The value of the concentration mixing length  $l_{c,m}$  within the mixing region between the injected flow and the initial boundary layer is assumed to be proportional to the height of the concentration mixing region

$$l_{c,m} = a_m W \tag{14}$$

where  $W = (y)_{G=0.99} - (y)_{G=0.01}$.  Few values of  $l_c/W$  deduced directly from experimental data are available; hence, the assumption is made that

$$a_m = \frac{l_u}{\delta_u} \tag{15}$$

which is evaluated from velocity data for two-dimensional mixing layers that simulate as closely as possible the present initial conditions for  g, that is, a step function with  $F = 0$  and  1.0  on the two sides of a splitter plate.  The assumption that  $\frac{l_c}{W} \approx \frac{l_u}{\delta_u}$  is based partly on the results of reference 46 (for axisymmetric jets of water), where by the method of Tollmien (ref. 47, p. 412), the concentration mixing length was  $\left(\frac{l}{r_{0.5}}\right)_c \approx 0.22$  and the velocity mixing length was  $\left(\frac{l}{r_{0.5}}\right)_u \approx 0.21$.  $\Big($The parameter  $r_{0.5}$   $\big($or  $y_{0.5}\big)$  is

a more reliable measure of the mixing-layer height than the total height of the mixing layer for free turbulent mixing with quiescent surroundings because of the asymptotic approach to zero velocity for this type of flow.) With this assumption, the value of the mixing length in the free-mixing region between the jet flow and the exterior flow is (from eqs. (7) and (14))

$$l_{u,m} = N_{Sc,T} a_m W \tag{16}$$

This procedure then provides calculated values of a velocity mixing length for the present slot-flow problems, where the initial velocity profiles are not uniform and, therefore, the values of $\delta_{u,m}$ cannot be determined directly from the velocity profiles.

To account for the effect of different scales in the outer boundary layer and the injected jet on the mixing length within the mixing region proper, the value of $l_{u,m}$ is assumed to apply only at the center of the mixing region, denoted by $y_{c,r} = y_{G=0.5}$ in figures 1(b) and 1(c). The method used to obtain the coordinates of the other "pivot" points for the mixing-length distributions in the three zones indicated in figure 1(c) will be presented in subsequent sections of this report.

Experimental values of the turbulent Schmidt number have been measured in subsonic slot-injection flows, as reported in reference 38, where it was concluded that $N_{Sc,T} = 0.5 \pm 0.2$ was representative of the majority of data points. Experimental values of $N_{Sc,T}$, given in reference 46, for axisymmetric air and water jets vary from 0.67 to 0.80. Also in reference 46, the value of the mixing-length ratio $l_u/l_c$ (which is $N_{Sc,T}$ in the present approach; see eq. (7)) was 0.81 as determined again by the method of Tollmien. The data for subsonic coaxial jets in reference 44 gave average values for $N_{Pr,T}$ of 0.6 and 0.85 for air-air and hydrogen-air mixing, respectively. As mentioned previously, these same data showed that $N_{Le,T} = 1.0$, which requires that $N_{Sc,T} = N_{Pr,T}$. The results given in references 14 and 38 for concentration profiles and effectiveness as calculated by the finite-difference method of reference 37 were in better agreement with data when a linear variation for $N_{Sc,T}$ was used (rather than constant $N_{Sc,T}$ of 0.5 or 1.0) that varied from 1.75 at the wall to 0.5 at the boundary-layer edge. Since this particular linear variation of $N_{Sc,T}$ is not representative of most data (ref. 38), it was speculated in reference 38 that the improved agreement with data obtained with this linear variation was caused by compensating errors in the mixing-length model. From these brief comments on turbulent Schmidt number, it is apparent that little justification exists for using a particular value or functional variation for $N_{Sc,T}$. For the present solutions, constant values of $N_{Sc,T}$ of 1.0 and 0.8 have been

used. The molecular Schmidt number, $N_{Sc}$ has been taken as 0.7. To be consistent with the assumption that $N_{Le,T} = 1.0$, the relation that $N_{Sc,T} = N_{Pr,T}$ should be used. However, in the present solutions, $N_{Pr,T} = 0.9$ was used throughout partly in an attempt to isolate the effect of changes in $N_{Sc,T}$ on mixing length, and partly because the value $N_{Pr,T} = 0.9$ is representative of typical values used in previous calculations. (See refs. 34, 35, and 37, for example.)

Values of $a_m$ used herein are based primarily on data obtained for two-dimensional, free turbulent mixing layers. Although these values are found to vary considerably, reasonable limits can be established from data on jets and wakes.

Thus, from the data of reference 48 for a half-jet, the average value of $\dfrac{l_u}{y_{F=0.99}} \approx 0.15$ for the stream side of the jet. The thickness of the low-velocity side of the half-jet to the $F = 0.025$ point was about 1.4 times larger than that of the stream side, and the average $l$ was smaller; therefore, $\dfrac{l_u}{y_{F=0.025}} \approx 0.06$ for this side (the $F = 0.025$ point is used to represent the "edge" of the low-velocity side of the jet because of the extremely gradual approach to $F = 0$ on this side of the jet). If the total thickness of the half-jet is taken as the sum of the $y_{F=0.99}$ and $y_{F=0.025}$ values used above, the average value for $a_m$ is $\dfrac{l_u}{\delta} \approx 0.05$ where $\delta$ is the thickness of the jet between the points where $F = 0.025$ and 0.99.

For the plane symmetric jet (ref. 49), the value of $\left(\dfrac{l}{y_{0.5}}\right)_u \approx 0.25$ if values near the center line and edge are excluded. For these data, the value of $\dfrac{y_{F=0.025}}{y_{0.5}} \approx 2.1$; therefore, $\dfrac{l_u}{y_{F=0.025}} \approx 0.12$ or $\dfrac{l_u}{\delta_{F=0.025}} \approx 0.06$.

For the two-dimensional wake-flow data of Townsend (see ref. 47, p. 394), an average value of velocity mixing length (from Tollmien's method) was $\dfrac{l_u}{y_{0.5}} \approx 0.4$. Therefore, $\dfrac{l_u}{\delta} \approx 0.1$, since $\delta = 2y_{F=0.99}$ and $\dfrac{y_{0.5}}{y_{F=0.99}} \approx 0.5$. This value of $l_u/\delta$ is in agreement with Schlichting's data for wake flow (ref. 50, p. 692) where $\dfrac{l_u}{\delta} \approx 0.09$ by the same method.

The values used for $a_m$ in the present solutions were generally in the range of 0.05 to 0.12. This range of values is based on the experimental results discussed

previously; that is, the upper limit is obtained from the symmetric jet data of reference 49 by assuming that $\dfrac{l_u}{y_{F=0.025}}$ applies directly to $l_c/W$ in the present slot flows, and the lower limit is based on the $l_u/\delta$ value for the total width of the half jet (ref. 48).

Mixing-length distribution at slot exit and across initial boundary layer.- The mixing-length distribution at the slot exit is based on established values for fully developed channel flows. In reference 51, for example, it was shown that a mixing-length distribution of the form

$$l = \kappa e^{\left(1-\frac{2y}{s}\right)} y \qquad \left(0 \leq y \leq \frac{1}{2} s\right) \qquad (17)$$

yielded accurate velocity profiles and friction-factor equations for fully developed pipe and two-dimensional channel flows $\left(\text{for pipe flows, } \frac{1}{2} s \text{ is replaced by the pipe radius, } r_w\right)$. For channel flows, values of $\kappa$ increased from 0.13 to 0.16 as the Reynolds number, based on the average velocity and the hydraulic diameter decreased from about $9 \times 10^5$ to $2 \times 10^4$. Also, equation (17) gives Prandtl's wall relation (eq. (4a)) for small y, with K increasing from about 0.35 to 0.43 for the variation in $\kappa$ noted previously.

For the present solutions, equation (17) is approximated by a simple two-step ramp function. For the near-wall region, the Prandtl slope is used (eq. (4a)) and in the center region of the jet, $l_j$ is assumed constant, as given by

$$\frac{2l_j}{s} = a_j \qquad (18)$$

where for the present solutions $a_j$ was assumed to be 0.14. This value is obtained from equation (17) evaluated at $y = \frac{1}{2} s$ with $\kappa = 0.14$. When the slot flow is fully developed turbulent channel flow, this factor could be varied with channel Reynolds number based on the results of reference 51. On the other hand, if the slot flow is believed to be laminar, the value of $a_j$ would presumably be reduced considerably.

The mixing-length distribution across the initial boundary layer is also a two-step ramp function with equations (4a) and (4c) used in the near- and far-wall regions, respectively. However, the limiting values of $y/\delta$ that are used for these relations in conventional boundary-layer calculations are not applied herein at the initial input station. Instead, the limiting value of $y/\delta$ is determined from the intersection of the straight lines given by equations (4a) and (4b).

The coordinates of the pivot points at the initial input station $x = x_0$ are then given as follows (see fig. 1(c)):

| Point | $y$ | $\ell$ |
|-------|-----|--------|
| ① | $\dfrac{s}{2K}\, a_j$ | $\dfrac{s}{2}\, a_j$ |
| ② | $s\left(1 - \dfrac{a_j}{2K}\right)$ | $\dfrac{s}{2}\, a_j$ |
| ③ | $y_{G=0.5}$ | $N_{Sc,T}{}^{a}{}_m\left(y_{c,f} - y_{c,n}\right)_{x_O}$ |
| ④ | $s + t + \dfrac{f_f \delta_O}{K}$ | $f_f \delta_O$ |

$$\text{(19)}$$

Possible alternative coordinates for point ③ that are more closely related to the slot geometry are

$$y = s + \frac{1}{2}t \quad \text{and} \quad \ell_{u,m} \approx 0.1t$$

While these coordinates for point ③ are not included in the present computer program, they can be utilized by appropriate adjustment of the input $g$ profile. Note that the relations for points ③ and ④ account, in an approximate fashion, for a finite thickness $t$ of the slot lip. The mixing-length distributions between the coordinate points given previously and in the following sections are taken as straight-line segments. It should also be noted that throughout the present method, the Van Driest wall-damping function (see eq. (3)) is used only as a modifying factor applied to the basic mixing-length relations. Since this damping function depends exponentially on the distance $y$ from the wall and $\tau_w$, this function would have little effect on the final mixing lengths used in the program except for small values of $y$ or when the density level is small.

Mixing-length relations for downstream flow field.- The entire slot-injection flow field from the initial development of the mixing region to the final relaxation of the flow to an undisturbed boundary layer is calculated by utilizing somewhat different mixing-length relations in three distinct streamwise zones of the flow that are indicated in figure 1(c). The relations used for mixing length in these three zones are assumed to depend on the relative values of $\ell_{u,m}$, $\ell_j$, and $\ell_b$.

The mixing length $\ell_b$ in the outer region of the boundary layer is intended to provide for a continuous adjustment of the initial input value of $\ell_f$ (determined from eq. (4c))

20

as the initial boundary layer mixes with the jet flow. The assumed scale for this purpose is $\delta - y_{c,n}$. Hence

$$l_b = f_{f,s}\left(\delta - y_{c,n}\right) \tag{20}$$

where $y_{c,n}$ is taken as $y_{G=0.01}$ for the present solutions and where $f_{f,s}$ is the same function used in equation (4b) except that the lower limit of the integrals for $\delta_{in}^*$ and $\theta_{in}$ is $y_{G=0.01}$ rather than $y = 0$.

With the basic relations for the mixing lengths $l_{u,m}$, $l_j$, and $l_b$ given, respectively, by equations (16), (18), and (20) (which are to be applied, respectively, to the mixing region, the jet flow, and the outer boundary layer), the next task is to specify the distribution of mixing lengths across the entire boundary layer and the streamwise development of this distribution. The streamwise development of the distribution in zones I and II (see fig. 1(c)) is controlled by the magnitude of $l_{u,m}$ relative to the neighboring values of $l_j$ and $l_b$. In zone III an alternate criterion based on the computed value of $C_{A,w}$ is also used. With the Prandtl mixing-length slope $K$ always applied at the wall and with $l_{u,m}$ applied at the center of the mixing region (y at $G = 0.5$), the y coordinates of the "pivot" points connecting the three values can then be specified by adopting appropriate scaling factors. The relative values of the mixing lengths are used as criteria to determine the extent of the three streamwise zones. These criteria and the coordinates of the corresponding pivot points, identified in figure 1(c), are presented in the next three subsections.

Zone I (initial mixing region): This zone is defined by the following inequality:

$$l_j \geq l_{u,m} < l_b \tag{21}$$

The y and $l$ coordinates of the pivot points are then as follows:

| Point | y | $l$ | |
|-------|---|-----|---|
| ① | $\dfrac{s}{2K} a_j$ | $\dfrac{s}{2} a_j$ | |
| ② | $s\left(1 - \dfrac{a_j}{2K}\right)\dfrac{\delta}{\delta_r}$ | $\dfrac{s}{2} a_j$ | |
| ③ | $y_{G=0.5}$ | $N_{Sc,T}{}^a m\left(y_{c,f} - y_{c,n}\right)$ | (22) |
| ④ | $\left(s + t + \dfrac{f_{f,s}\delta_0}{K}\right)\dfrac{\delta}{\delta_r}$ | $f_{f,s}\left(\delta - y_{G=0.01}\right)$ | |

where $\delta_r = \delta_0 + t + s$. The y coordinates of pivot points ② and ④ include the factor $\delta/\delta_r$ in order to maintain the ratio of $y/\delta$ the same as the initial values for these points from relations (19). The use of this factor is suggested by standard procedure in boundary-layer calculations where $l/\delta$ is often assumed to be a function only of $y/\delta$. (See refs. 34 and 37, for example.)

Zone II (intermediate mixing region): This zone is defined by the inequality

$$l_j \lesssim l_{u,m} \lesssim l_b \tag{23}$$

The coordinates of the pivot points are then

| Point | y | $l$ |
|-------|---|-----|
| ① | $\dfrac{N_{Sc,T^a m}}{K}\left(y_{c,f} - y_{c,n}\right)$ | $N_{Sc,T^a m}\left(y_{c,f} - y_{c,n}\right)$ |
| ③ | $y_{G=0.5}$ | $N_{Sc,T^a m}\left(y_{c,f} - y_{c,n}\right)$ |
| ④ | $\left(s + t + \dfrac{f_{f,s}\delta_0}{K}\right)\dfrac{\delta}{\delta_r}$ | $f_{f,s}\left(\delta - y_{G=0.01}\right)$ |
| ④' | $\left(s + t + \dfrac{f_{f,s}\delta_0}{K}\right)\dfrac{\delta - y_{G=0.5}}{\delta_0} + y_{G=0.5}$ | $f_{f,s}\left(\delta - y_{G=0.01}\right)$ |

$$\tag{24}$$

where point ④' is a possible alternate form for point ④. It can be seen that in this intermediate mixing region, the reference mixing length $l_{u,m}$ is still applied at the center of the free-mixing region, but also is extended toward the wall to intersect with the Prandtl slope and thereby account for the increasing influence of the entire boundary layer on the wall region. Also, the alternate form for y at point ④' could be used when $s \ll \delta_0$ and y at point ③ could then exceed y at point ④ in zone II.

Zone III (approach and relaxation to final equilibrium boundary layer): The criteria that control the change to the final mixing-length relations used in this zone are based on either the final relaxation of mixing-length relations, as given by the inequality

$$l_j \lesssim l_{u,m} \gtrsim l_b \tag{25}$$

or by the computed wall concentration according to the relation

$$C_{A,w} \geq 0.85 \tag{26}$$

This latter inequality is assumed to apply during the final stages of mixing, and the 0.85 factor was used herein to represent the beginning of this condition. Tests are applied continuously toward the end of the solution and in the present computer program (see appendix), whichever of these relations (25) or (26) is satisfied first is used as the criterion to start applying the following coordinates:

| Point | $y$ | $l$ |
|-------|-----|-----|
| ① | $0.1\delta$ | $K(0.1)\delta$ |
| ④ | $0.3\delta$ | $f_{f,s}\delta$ |

$$(27)$$

Thus, in this last zone, essentially the same relations are used that would be applied to a conventional undisturbed boundary layer. (See eqs. (4).) The slight difference between the limits used for $H^*_{in,s}$ and $H^*_{in}$ is of little consequence in this zone. Since this zone should account for the final adjustment of the boundary layer to its undisturbed "state," the values of $C_{A,w}$ should approach free-stream values somewhere in zone III. Depending on the choices of $a_m$ and $N_{Sc,T}$, criterion (25) may or may not be satisfied before $C_{A,w} \rightarrow 1.0$.

## APPLICATION OF METHOD AND DISCUSSION OF RESULTS

In this section, theoretical predictions for velocity profiles, heat transfer, and effectiveness will be compared with experimental data downstream of tangential injection from references 21 to 24 and 29. Also, theoretical predictions of skin friction will be compared with data obtained by Aubrey M. Cary, Jr., at the Langley Research Center with the same apparatus as described in reference 29.

The slot configurations used in the investigations of references 21, 22, and 29 consisted of convergent or constant-area channels, so that essentially sonic velocities were obtained at the exit of the slots. The velocity at the slot exit was supersonic in the investigation of reference 24. Experimental data were generally available at the slot exit or slightly downstream of the exit, and these data were used as the initial inputs for the solutions.

### Comparisons With Velocity Profile Data at Mach 3.0 for Adiabatic Injection

The first two test cases to be considered are taken from data of reference 21 and computed profiles of velocity, concentration, and mixing-length distribution will be shown

in some detail for these cases.  The free-stream Mach number was 3.0, and the slot walls were inclined $15^O$ to the surface of a flat-plate model.  The value of  t  was taken as 0.0025 cm (0.001 inch).  The temperatures of the free-stream and jet flows and of the surface were such that the flow was essentially adiabatic, and velocity-profile data were obtained at seven stations from the slot exit to $\frac{\Delta x}{s} \approx 235$.  Since the only experimental data available for these flows are the velocity profiles and skin-friction coefficients, the theoretical results for concentration and mixing length are included mainly to illustrate how these parameters influence the computations for realistic flow conditions.

Large slot height, $\frac{s}{\delta_O} \approx 0.95$
.- This test case is the rearward-inclined step slot flow reported in reference 21 with  s = 1.7 mm (0.068 inch).  Theoretical calculations and experimental results for  F  and  $\delta$  for the seven stations are shown in figure 2. Also shown are the computed distributions for  G,  $l$,  and  $y_{c,f}$  (G = 0.99),  $y_{G=0.5}$,  and $y_{c,n}$  (G = 0.01).  Results from three solutions are presented to indicate the effect of changes in the mixing-length parameter  $a_m$  and in the turbulent Schmidt number  $N_{Sc,T}$. The criterion used in these solutions to control the changeover to the equilibrium mixing lengths of relations (27) was that of inequality (25) only.

The input velocity at the slot lip (see fig. 2(a)) is not zero because the input profile was assumed to apply at some small distance downstream of  $x_O$.  Thus, while the input profile was based on available data, as indicated, a finite value of  F = 0.3  was used at the slot lip (y = 1.7 mm (0.068 inch)) rather than zero which would be required to satisfy the no-slip boundary condition on the slot lip itself.  Even with this apparent increase in velocities in the vicinity of the slot lip, the integrated mass flow from  y = 0  to  y = s was only 0.0154 kg/sec (0.034 lb/sec) which is about 10 percent smaller than the quoted experimental value of 0.0172 kg/sec (0.038 lb/sec).  This discrepancy in theoretical and experimental injected mass-flow rates is probably due to some excess in static pressure at the slot exit compared with the local free-stream static pressure, as may be inferred from data given in reference 21.

Comparison of the predicted and experimental velocity profiles in figures 2(a) and 2(d) shows that solution 2 with the smallest value of  $a_m$  gives the smallest values of velocity which are in the best agreement with data for  $x \geq 11.05$ cm (4.35 inches).  The smaller velocities in solution 2 resulted from the smaller value of  $a_m$, which caused smaller values of mixing length, as shown in figures 2(c) and 2(f).  In fact, for this solution the mixing-length relations were such that  $l_{u,m} < l_b$  throughout, therefore, zone III (see fig. 1) was never attained in this solution since criterion (26) was not used.  At x = 10.05 cm (3.95 inches), solution 1 gave the best agreement with the data, whereas at x = 8.96 cm (3.53 inches)  solution 3 gave better agreement.  In view of the difficulties

involved in obtaining accurate profile data in a boundary layer 2.5 to 5.1 mm thick (0.1 to 0.2 inch), all three solutions are considered to be in satisfactory agreement with the data.

The G profiles and edges of the mixing region are shown in figures 2(b) and 2(e). Comparison of results from the three solutions shows that solution 2 $\left(\text{with } a_m = 0.06\right.$ and $\left. N_{Sc,T} = 1.0\right)$ gave the smallest values of G at the first two stations downstream of the lip. However, at the last three stations, this solution gave larger values of G apparently because of the significant reductions in both F and G boundary-layer thicknesses for $x > 12.7$ cm (5.0 inches). These smaller boundary-layer thicknesses are again caused by the smaller values of mixing length for solution 2.

It is of interest to point out similarities between the computed shape and distribution of the concentration mixing region, as given by the values of $y_{c,f}$ and $y_{c,n}$ in figure 2 with the corresponding edges of the mixing region from velocity data of reference 9. The experimental coordinates of the upper and lower edges of the mixing region resulting from tangential slot injection into a flow with a thin initial boundary layer were shown in this reference. For $\frac{u_j}{u_e} \leq 0.36$ and $\frac{\Delta x}{s} < 10$, the inclination or angle of the lower edge was considerably greater than that of the upper edge. This same trend is apparent in the theoretical results shown in figure 2(b). Also the location of an effective origin of the velocity mixing region (determined by upstream extrapolation of the linear part of the edges) in the data of reference 9 was located slightly upstream and above the slot rather than at the slot lip itself. This same general shift in the effective origin of the mixing region is also apparent from the results for $y_{c,f}$ and $y_{c,n}$ shown in figure 2(b).

The locations of the three mixing-length zones defined in figure 1 are indicated in figure 2(c) for these solutions. It is seen that the values of $a_m$ have a marked effect on the location of the changeover points from one zone to the next. Thus, while the best agreement with the downstream velocity profiles was obtained with solution 2, the failure of this solution to reach zone III or final equilibrium mixing-length distributions even at the last station $\left(\frac{\Delta x}{s} = 235\right)$ is probably an indication that either $a_m$ was too small or the alternate criterion (26) should have been used. In this connection, it is of interest to compare the values of $C_{A,w}$ from the three solutions at $x = 20.3$ and 49.0 cm (8.0 and 19.0 inches) given in the following table:

| Solution | $a_m$ | $N_{Sc,T}$ | $C_{A,w}$ at x in cm (in.) equal – | |
|---|---|---|---|---|
| | | | 20.3 (8.0) | 49.0 (19.3) |
| 1 | 0.09 | 0.8 | 0.81 | 0.93 |
| 2 | .06 | 1.0 | .73 | .90 |
| 3 | .10 | 1.0 | .78 | .92 |

Again, $C_{A,w}$ values for solution 2 are the smallest, whereas the values for the other two solutions approach unity more rapidly; this trend indicates that the predicted mixing process is faster for solutions 1 and 3. Thus, the $C_{A,w} = 0.85$ criterion of inequality (26) was attained first in solution 1. This result is believed to be the most realistic because the experimental velocity profile shapes were nearly the same as those for the undisturbed flat plate (see comparisons in ref. 21) by, at least, the $x = 36$ cm (14.0 inches) station. Hence, the values of $a_m$ and $N_{Sc,T}$ used in solution 1 have been selected as reasonable compromise values and will be used in all remaining solutions, partly on the basis of the $C_{A,w}$ behavior and partly because of the good agreement with velocity profiles from this solution and the data for the first two stations in the critical region of $\frac{\Delta x}{s} < 10$. Also, the changeover criterion given by inequality (26) will generally be used in the remaining solutions.

Small slot height, $\frac{s}{\delta_0} \approx 0.20$.- This test case was also taken from reference 21 but for the rearward step slot with $s = 0.38$ mm (0.015 inch). The predicted $F$ and $G$ profiles and the mixing-length distributions are shown in figure 3. The mixing-length ratios used in this solution were $a_j = 0.14$ and $a_m = 0.09$ and the turbulent Schmidt number was $N_{Sc,T} = 0.8$. The experimental velocity-profile data are also shown in the upper part of the figure.

Since the quoted value of injected mass flow was 0.0172 kg/sec (0.038 lb/sec), the same as for the large-slot-height test with $s = 1.7$ mm (0.068 inch), the experimental injection pressure would have to be increased by the ratio of $s$ values or by about 4.5. Hence, the velocities just downstream of the lip would be considerably larger than sonic because of the sudden expansion of the slot flow. The input-velocity profile is again based on experimental values which do indicate (fig. 3(a)) that a large and sudden expansion apparently took place just aft of the lip as evidenced by the outward displacement of the jet flow and the large ratio of jet to external velocities of about 0.8 at the first station. Since the external Mach number was 3.0, the injected jet flow was supersonic at about Mach 2.4 at this first station. Since the injection channel was constant area or convergent, the pitot probe would therefore have been slightly downstream of the lip. With the present theoretical restriction of constant static pressure, the integrated theoretical injected mass flow was only 0.0099 kg/sec (0.022 lb/sec) or about 40 percent lower than the experimental value.

In spite of this discrepancy in injected mass-flow rates, the computed velocity profiles are considered to be in reasonable agreement with the data. This acceptable agreement indicates that reasonable predictions of velocity distributions can be obtained even when the static pressure and angle of the injected flow deviate considerably from the

theoretical assumptions involved in the boundary-layer equations; providing initial profiles are available.

The mixing-length distributions shown in figure 3 indicate that zone III (and the associated final equilibrium mixing lengths) was reached upstream of the station where $x = 20.4$ cm (8.05 inches) in this solution. Actually, the criterion of $C_{A,w} = 0.85$ was reached at $x = 20.3$ cm (8.00 inches), just slightly upstream of the station where profiles are shown. This corresponds to $\frac{\Delta x}{s} = 310$ and $\frac{\Delta x}{\delta} \approx 40$, either of which seems a physically reasonable distance to begin the approach to an equilibrium boundary layer. For the conditions of this solution, the mixing-length criterion (25) was never reached even at $x = 49.0$ cm (19.3 inches) $\left(\frac{\Delta x}{s} = 1060 \text{ or } \frac{\Delta x}{\delta} \approx 90\right)$, which is probably an excessive distance to reach equilibrium. Hence, for situations like this one, where $s \ll \delta_0$, criterion (26) is thought to provide more realistic results.

Skin-friction predictions and comparisons with experimental data.- The calculated distributions of skin friction for $s = 0.38$ mm and 1.7 mm (0.015 and 0.068 inch) are compared with experimental data from reference 21 in figure 4. At $x = 50.8$ cm (20 inches), data were obtained with a skin-friction balance on the solid plate (no slot) and for both rearward-inclined step slots of $s = 0.38$ and 1.7 mm (0.015 and 0.068 inch). These data showed that the 1.7-mm (0.068-inch) slot caused a 5-percent increase in skin friction while the 0.38-mm (0.015-inch) slot caused a 3-percent decrease. The other data for zero injection are based on measured values of $\theta$. Comparison of the theoretical predictions with these no-injection data indicate that injection reduces the skin friction over the entire plate for both slot heights. The greatest reductions were predicted for the 1.7-mm (0.068-inch) slot. Significant reductions were also predicted for the smaller slot, but only up to $x \approx 10.16$ cm (4 inches) or $\frac{\Delta x}{s} \approx 40$. The magnitude of actual reductions in $C_f$ that may be realized for mismatched pressure conditions like those for the smaller slot should probably be determined from experimental data since the expansion or compression wave systems would probably modify the present velocity profiles considerably.

## Comparisons With Heat-Transfer Data at Mach 6 for $\frac{T_{t,j}}{T_{t,e}} \approx 0.66$

Sonic injection velocities.- The next test case to be considered is based on data from references 22 and 23. The model was an axisymmetric center body mounted on the center line of an axisymmetric Mach 6 contoured nozzle. The diameter of the model in the test region was 11.74 cm (4.623 inches) and the initial boundary-layer thickness just ahead of the slot was about 2.03 cm (0.8 inch). The data to be used here were obtained with a rearward-facing tangential slot of 0.25-mm (0.01-inch) height. The area

distribution of the approach channel to the injection slot was convergent, so the injection velocity was sonic.

The mass-injection ratio $\lambda$ was varied from about 0.06 to values greater than unity by increasing the injection pressure. The mass-injection ratio is defined herein as

$$\lambda = \left( \frac{1}{s} \int_0^s \frac{\rho}{\rho_e} F \, dy \right)_{x_o} \tag{28}$$

In terms of an average mass ratio,

$$\lambda_{av} = \left( \frac{\rho_{j,o} u_{j,o}}{\rho_e u_e} \right)_{av}$$

where $\lambda_{av} \approx \lambda$, the ratio of the static pressure at the slot exit to the local-stream static pressure is

$$\frac{p_{j,o}}{p_e} = \frac{M_e}{M_{j,o}} \left( \frac{1 + \frac{\gamma - 1}{2} M_e^2}{1 + \frac{\gamma - 1}{2} M_{j,o}^2} \frac{T_{t,j,o}}{T_{t,e}} \right)^{1/2} \lambda_{av} \tag{29}$$

Then with the conditions of references 22 and 23 $\left( M_j = 1.0, \quad M_e = 6, \text{ and } \frac{T_{t,j,o}}{T_{t,e}} \approx 0.66 \right)$,

$$\frac{p_{j,o}}{p_e} \approx 12.7 \lambda_{av} \tag{30}$$

and in order to satisfy the present limitation of constant static pressure the value of $\lambda_{av}$ should be about 0.08.

The input profiles used in the solutions are shown in figure 5. These profiles are based on data given in reference 23 for $y \gtrsim 0.25$ mm (0.01 inch). The profiles in the slot region were adjusted to give $\lambda = 0.068$ so as to satisfy approximately the requirement of $\frac{p_{j,o}}{p_e} \approx 1.0$ from equation (30). All data reported in references 22 and 23 were obtained with $T_w$ approximately constant at room temperature. Hence, $\frac{T_w}{T_{t,e}} = 0.66$ represents the mean of the experimental range in $T_{t,e}$ of $400^\circ$ K ($720^\circ$ R) to $500^\circ$ K ($900^\circ$ R). A solution designated in the following discussion as the "heat-transfer solution" was then obtained with $\frac{T_w}{T_{t,e}} = 0.66$.

The predicted heat-transfer distribution from this solution is plotted in figure 6 in terms of the correlating parameters from reference 22 $\left[1 - \left(\dot{q}_W/\dot{q}_{W,r}\right)\right]$ and $X = \frac{\Delta x}{s}(\lambda)^{-0.8}$. The reference heating-rate values $\dot{q}_{W,r}$ were computed from the same reference-enthalpy expression used in reference 22:

$$N''_{St,r} = \frac{\dot{q}_{W,r}}{\left(T_{aw} - T_W\right)\rho''u_e c_p} = \frac{0.0296}{\left(N''_{Re}\right)^{0.2}\left(N_{Pr}\right)^{2/3}} \tag{31}$$

where

$$T_{aw} = \omega\left(T_{t,e} - T_e\right) + T_e \tag{32}$$

and $\omega = 0.89$ was used herein to obtain $\dot{q}_{W,r}$. The gas-property values in equation (31) are evaluated at the reference temperature (ref. 22)

$$T'' = 0.5T_W + 0.22N_{Pr}^{1/3}\left(0.5 - 0.22N_{Pr}^{1/3}\right)T_{t,e} \tag{33}$$

It was stated in reference 22 that the measured heating rates for zero injection were within 10 percent of the values from equation (31), so the computed values of $\dot{q}_{W,r}$ are consistent with the experimental values.

Also shown in figure 6 are the experimental data (shown as the hatched band) and the straight line which correlated the data in reference 22 for $X > 200$. The predicted heat-transfer distribution is within the spread of the data for $150 < X < 600$. The predicted results are greater than unity for $X < 150$ because the input wall temperature of $T_W = 294^O$ K ($530^O$ R) was larger than the effective recovery temperature in this region and therefore the calculated heating was negative (heat transfer from the wall to the flow). The disagreement between predictions and data for $X > 600$ is probably within the experimental uncertainty band of the data. At $X = 800$, for example, the theory predicts a heating rate that is only 4 percent larger than the largest measured value. (Some of the spread in the data may be caused by different values of $\lambda$; however, the values of $\lambda$ for the original data points in reference 22 were not identified.)

A parameter of particular interest in the application of slot-cooling techniques is the effectiveness, which is defined in reference 22 as

$$\eta = \frac{T_{t,e} - T_{aw}}{T_{t,e} - \overline{T}_{t,j,o}} \tag{34}$$

It can be seen that $\eta$ provides a measure of the thermal protection afforded by injection since values of $\eta$ near 1 indicate that the local recovery temperature at the wall is still close to the jet total temperature. However, since the recovery temperature for the jet flow may be less than the jet total temperature, the values of $\eta$ from equation (34) could exceed unity.

Values of $T_{aw}$ and hence $\eta$ are computed in the present method by replacing the boundary condition $H_w(x)$ (see ref. 41) by $\left(\dfrac{\partial H}{\partial y}\right)_w = 0$. The value of $H_w$ required to satisfy the new boundary condition is then computed directly from the differential equation for $\zeta$. Since the surface heat transfer is zero when $\left(\dfrac{\partial H}{\partial y}\right)_w = 0$, the resulting values of $\zeta_w = \dfrac{T_{aw}}{T_{t,e}}$ for constant $c_p$. Details of this procedure, which is also used to determine $C_{A,w}$ with boundary condition (10b), are presented in the appendix.

Another solution, designated the "adiabatic-wall solution," was obtained with this procedure for computing $T_{aw}$ but with all other input and boundary conditions identical to those of the heat-transfer solution. The resulting values of $\eta$ are plotted against the correlating parameter X in figure 7. Shown for comparison in the figure are the experimental data and straight-line correlation from reference 22. The computed values of $\eta$ from the adiabatic-wall solution are considerably larger than the experimental values of $\eta$ for X > 200; hence, the computed recovery temperatures are smaller than those used in reference 22. As mentioned previously, the values of $T_{aw}$ used in reference 22 to determine $\eta$ were calculated by utilizing measured values of $\dot{q}_w$ in equation (31). When this same procedure for computing $\eta$ is applied to predicted values of $\dot{q}_w$ from the heat-transfer solution $\left(\text{obtained with } \dfrac{T_w}{T_{t,e}} = 0.66\right)$, the $\eta$ distribution, shown as the dashed line in figure 7, is obtained. As would be expected, this distribution of $\eta$ is in agreement with the data since the predictions for $\dot{q}_w$ agreed with the data.

The values of $T_{aw}/T_{t,e}$ computed directly in the adiabatic-wall solution and computed from equation (31) with $\dot{q}_w$ from the heat-transfer solution are shown in figure 8. The latter procedure yields values of $T_{aw}/T_{t,e}$ that are at most 13 percent larger than values computed directly in the former solution. The maximum difference in temperature is about $44^O$ K ($80^O$ R), which can be easily measured in a facility with long test times. The larger values of $T_{aw}/T_{t,e}$ are questionable because even for a simple flat-plate flow, it is known that equation (31) is not correct when $dT_w/dx$ is sufficiently large. (See refs. 31 and 32.) In the present situation, the wall temperature increases by about $83^O$ K ($150^O$ R) in a distance of 2.5 to 5.1 cm (1 to 2 inches). Also, the injection and

mixing of a cold layer of air near the surface would cast further doubt on the use of equation (31) to compute $T_{aw}$. Of course, direct measurements of $T_{aw}$ are required to verify the theoretical predictions of the adiabatic-wall solution, which indicate that $T_{aw}$ may not reach the nominal equilibrium values until $\Delta x/s$ exceeds several thousand. Such measurements are available (ref. 29) and will be compared with predictions in a subsequent section.

As a matter of interest, the computed values of $C_{A,w}$ from the heat-transfer solution are shown in figure 8. Again the final equilibrium value for $C_{A,w}$ of unity may not be reached until $\dfrac{\Delta x}{s} > 2000$ to 3000.

Supersonic injection velocities.- Surface heat-transfer measurements are reported in reference 24 for supersonic injection from a tangential slot into a 2.54-cm-thick (1-inch) turbulent boundary layer. The free-stream test conditions and the model configuration were the same as those of reference 22 except the slot height $s$ was 5.6 mm (0.22 inch) and the injection velocity was supersonic at $M_j \approx 2.3$. Accordingly, the theoretical solution for these conditions was obtained with the same initial profiles for $F$ and $\zeta$ shown in figure 5 except the maximum velocity ratio at the jet exit was increased to 0.617 $\left(\text{corresponding to values quoted in ref. 24 of } M_j = 2.3, \dfrac{T_t}{T_{t,j,o}} = 0.66, \text{ and}\right.$

$\left. M_e = 6.25 \right)$ and $s$ was increased to 5.6 mm (0.22 inch).

The predicted heat-transfer distribution in the form of $1 - \dfrac{\dot{q}_w}{\dot{q}_{w,r}}$ is plotted against X in figure 9. The value of $\dot{q}_{w,r}$ was again computed from equation (31) with the same stream conditions and $\omega = 0.89$ as used for the previous case. The experimental data from reference 24 are also shown in the figure as the hatched area. Data points for $\lambda_{av}$ from 0.139 to 0.248 are included. The theoretical prediction is near the upper edge of the hatched data band. However, all data points, except one, in the range of $\lambda_{av}$ of 0.139 to 0.248 are near the upper edge of the shaded band in figure 9. Since $\lambda = 0.2$ was used in the solution, the agreement between predicted results and data is reasonable.

### Comparisons With Recovery Temperature and Skin-Friction Data at Mach 6 for $\dfrac{T_{t,j}}{T_{t,e}} \approx 0.65$

The data considered in this section are from reference 29 where direct measurements of $T_{aw}$ downstream of a two-dimensional tangential slot were reported. The

free-stream Mach number was 6.0, the free-stream and jet total temperatures were approximately 472° K (850° R) and 289° K (520° R), respectively, the exit velocity at the slot was sonic, and the initial turbulent boundary layer just upstream of the slot was about 5.1 cm (2 inches) thick. The ratio of measured slot mass-flow rate to calculated free-stream mass-flow rate was varied from 0.06 to 1.6, corresponding to pressure ratios of $\dfrac{p_{j,o}}{p_e} \approx 0.8$ to 20 from equation (29). The model was mounted on the floor of the Langley 20-inch Mach 6 tunnel.

The initial profiles used for the solution are shown in figure 10. The $F$ and $\zeta$ profiles are based on both the experimental data obtained on the wind-tunnel floor without the slot present and on the indicated experimental values of $T_{w,o}/T_{t,e}$, s, and t. While the profiles at the slot exit were not measured, they are based on known properties of channel flow. The shape and level of the $\zeta^{\cdot}$ profile at the slot exit represents an attempt to satisfy measured boundary conditions on the upper surface of the channel and a short distance upstream of the slot exit. Also, the value of $T_{t,j,o}/T_{t,e}$ used to calculate $\eta$ was 0.65 rather than about 0.61 as used to reduce the data in reference 29. This larger value of $T_{t,j,o}/T_{t,e}$ was used herein because of increased values of $T_{t,j,o}$ measured recently by Cary in the jet exit. These larger values of $T_{t,j,o}$ were apparently caused by heat conduction through the steel lip of the slot. The integrated slot mass-flow ratio for the profiles shown was $\lambda = 0.065$ which corresponds approximately to a matched pressure condition where $\dfrac{p_{j,o}}{p_e} \approx 1.0$ in accordance with this limitation of boundary-layer theory.

The computed distribution of effectiveness $\eta$, defined by equation (34), is plotted in figure 11 against the same correlating parameter $X$ used previously. The experimental data from reference 29 are shown as the hatched band. Agreement between the prediction and data is good over the entire range of the measurements up to $X \approx 800$, although the prediction is somewhat higher than the data for $100 < X < 200$. The generally good correlation of the data with the parameter $X$ for the large range of experimental mass ratios from $\lambda = 0.06$ to 1.6 indicates that the corresponding range of jet-to-stream pressure ratios of $\dfrac{p_j}{p_e} \approx 1.0$ to 20 has little effect on recovery temperatures. From the good agreement between the theoretical prediction and the data, it follows that for this range of conditions, the surface temperatures are determined mainly by the turbulent mixing phenomena as predicted by the present boundary-layer theory.

The correlation from reference 22 is also shown for comparison in figure 11. At large values of the correlating parameter $X$, the effectiveness from the direct measurements of reference 29 and as predicted by the present theory is as much as 100 percent

larger than the correlation of reference 22. These results show that $T_{aw}$ cannot be computed simply from measured heating rates and flat-plate heat-transfer relations.

Direct measurements of skin friction have also been obtained recently by Cary at three stations downstream of the slot on the same model used for the recovery-temperature data of reference 29. Skin-friction balances similar to those described in reference 52 were used to obtain these new data. Predicted values of $C_f$ from the solution are compared with the data in figure 12. The agreement is good, in spite of the large lip thickness $(t/s = 1/3)$ used in the experiment. Two more or less compensating effects may be present in this experiment. These are a possible low turbulence level in the slot flow caused by the very short approach configuration with its large accelerations (see ref. 53) and the thick lip which presumably would tend to increase turbulence levels downstream of injection. These effects can be roughly accounted for in the present theory by adjustment of the initial velocity profile in the slot and by using different values of $a_j$. Such adjustments are not warranted without data that would be required to incorporate properly these effects of turbulence level on the mixing-length models.

Also included in figure 12 are measured values of skin friction on the tunnel wall without the slot. These measurements were obtained with the same instruments, at the same $x$ locations, and for the same free-stream conditions as the slot-injection data. Comparisons between these data and the data with injection show that the skin friction is reduced significantly by slot injection under these conditions up to $\Delta x/s$ values of at least 70. An average reduction of approximately 60 percent is attained in the near-slot region of $\frac{\Delta x}{s} < 20$. It is also concluded that reliable predictions of level and trends in skin friction are obtained from the finite-difference solutions with the present mixing-length equations and constants.

## CONCLUDING REMARKS

An implicit finite-difference method has been used to solve the partial differential equations for compressible turbulent boundary layers with tangential slot injection. The turbulent-flux terms have been modeled with eddy-diffusivity and mixing-length concepts. The species-conservation equation is used to calculate the concentration field, which, in turn, is utilized to provide appropriate scales and criteria for different mixing-length models applied in three different zones downstream of the injection slot. When the primary and secondary flows are homogeneous, as in the example problems treated herein, the species conservation equation governs the spread of a "trace" species which has no direct effect on the velocity and enthalpy fields, but which serves to define the center and edges of the free-mixing region. The mixing lengths for this species concentration field are related to velocity mixing lengths by the turbulent Schmidt number.

Predictions for velocity profiles, heat transfer, effectiveness, and skin friction have been compared with experimental data from four different investigations at stream Mach numbers of 3.0 and 6.0 with sonic and supersonic injection velocities. These comparisons show that the turbulent-flux models developed herein provide realistic predictions for the entire flow from the near-slot region through the final relaxation region even when the boundary-layer limitation of small normal-pressure gradients is violated. This limitation was violated in various degrees in most of the experimental data considered herein because of such factors as mismatched pressures at the jet exit, finite injection angle, and thick slot lip.

An indirect procedure used by previous investigators for calculating the recovery temperatures from measured heating rates and flat-plate-correlation equations for heat-transfer coefficients underestimates the thermal effectiveness of tangential slot injection in hypersonic flows by significant amounts. The flat-plate-correlation equations cannot be used in this way because the relaxation process to undisturbed equilibrium conditions is slower for recovery temperatures than for heat-transfer rates.

Langley Research Center,
    National Aeronautics and Space Administration,
        Hampton, Va., March 2, 1971.

# APPENDIX

## MODIFICATIONS TO NONSIMILAR BOUNDARY-LAYER PROGRAM FOR
## COMPUTATION OF SLOT-INJECTION FLOWS

By Barbara A. Hixon and Dennis M. Bushnell
Langley Research Center

The compressible turbulent boundary-layer computer program described in reference 41 has been modified for application to tangential-slot-injection flows. The purpose of this appendix is to describe these modifications so that the program as presented in reference 41 can be used to compute relaxing tangential-slot flows at matched exit-pressure conditions. The program can be run with either the adiabatic-wall boundary condition or a specified wall temperature and wall-temperature gradient. If ZETWTAB $\left(\zeta_w \text{ table}\right)$ and DZDXTAB $\left(d\zeta_w/dx/dL\right)$ (see ref. 41) are given as input, they will be used; otherwise the program utilizes the adiabatic-wall boundary condition. The spanwise or g-momentum equation of reference 41 has been used herein as a species-conservation equation (eq. (9)). Therefore, it was necessary to discontinue treating g as a velocity term (as was done in ref. 41).

For convenience the complete program listing is given. Portions of the program which differ from that in reference 41 are indicated on the listing. The reason for a modification is generally identified as being one of the following:

$\textcircled{1}$ Additional input and output statements

$\textcircled{2}$ Changes in eddy-viscosity expression to account for slot and mixing-region flows

$\textcircled{3}$ Logic used in computation of adiabatic- and impermeable-wall boundary conditions

The extra input $\left(\text{indicated by } \textcircled{1}\right)$ is necessary to compute the concentration profile, the various pivot points associated with the mixing length for the slot and mixing-region flows, and the mixing-length predictions.

The changes due to the eddy-viscosity function $\left(\text{indicated by } \textcircled{2}\right)$ are necessary to compute the relaxing slot flow and are discussed in the text of the present report.

To apply the correct boundary condition on the concentration profile for an impermeable wall (zero gradient at the wall, eq. 10(b)), the solution must be obtained in terms

of the concentration directly. The algorithm for the computation of the g quantity (treated herein as species concentration) is, in the notation of reference 41,

$$g_n = \hat{G}_n g_{n+1} + \hat{g}_n \tag{A1}$$

where $\hat{G}_n$ and $\hat{g}_n$ are the recursion functions. Since n = 1 corresponds to the wall value, the impermeable-wall boundary condition requires that

$$g_2 = g_1$$

and therefore from equation (A1)

$$g_1 = \hat{G}_1 g_1 + \hat{g}_1$$

This result can only be correct for arbitrary $g_1$ if $\hat{G}_1 = 1$ and $\hat{g}_1 = 0$. These values are then used in the recursion relations for $\hat{G}$ and $\hat{g}$ at n = 2 (the first step away from the wall), with the result (see eq. (31) in ref. 41).

$$\hat{G}_2 = \frac{-\hat{A}_2}{\hat{B}_2 + \hat{C}_2} \quad \text{and} \quad \hat{g}_2 = \frac{\hat{D}_2}{\hat{B}_2 + \hat{C}_2} \tag{A2}$$

In the notation of reference 41, the $\hat{A}$, $\hat{B}$, $\hat{C}$, and $\hat{D}$ quantities are coefficients in the general difference equation for g. The values for $\hat{G}_2$ and $\hat{g}_2$ obtained from equations (A2) are used to compute the $\hat{G}_n$ and $\hat{g}_n$ quantities (ref. 41) and the zero-gradient boundary condition at the wall (eq. 10(b)) is then satisfied.

When the adiabatic-wall temperature is required, the solution is obtained in terms of $\zeta$ instead of $\overline{\Theta}$ so that again the boundary condition of equation 10(d) can be applied directly by the same procedure used for the concentration. These changes are indicated by ③.

The following is a list of nomenclature added to the program described in reference 41:

Input:

| Program notation | Report notation | Description |
|---|---|---|
| A1 | $a_j$ | Mixing-length ratio for center of initial slot flow, recommended value, 0.14 |
| A2 | $a_m$ | Mixing-length ratio for free-mixing region, recommended value, 0.09 |

| Program notation | Report notation | Description |
|---|---|---|
| SM | $N_{Sc}$ | Molecular Schmidt number |
| SNT | $N_{Sc,T}$ | Turbulent Schmidt number, should be approximately same as turbulent Prandtl number, recommended value, 0.8 |
| TDL | $t/L$ | Nondimensional slot-lip thickness |
| XXL1 | $(x/L)_1$ | Nondimensional distance at beginning of $x$ step during solution |
| XXL2 | $(x/L)_2$ | Nondimensional distance at end of $x$ step during solution |
| YCDL | $s/2L$ | Nondimensional distance to center of slot |
| YDD0 | $\dfrac{s+t}{\delta_0} + \dfrac{f_f}{K}$ | Initial nondimensional distance to pivot point number ④ (see eqs. (19)) |
| YDEL | $\delta$ | Local boundary-layer thickness (value of $y$ where $F = 0.995$) |
| YDEL0 | $(s + t + \delta_0)/L$ | Initial nondimensional boundary-layer thickness (for entire flow) |
| ∅L | $L$ | Reference length, generally 1 cm or 1 inch |

Output:

| | | |
|---|---|---|
| YDLG | $y_{c,r}/L$ | Nondimensional height to $G = 0.5$ location |
| YS1DL | $y_{c,n}/L$ | Nondimensional height to $G = 0.01$ location |
| YS2DL | $y_{c,f}/L$ | Nondimensional height to $G = 0.99$ location |

A complete listing of the program for slot-injection flows, with changes to the program of reference 41 identified, is now presented.

```
PROGRAM D2630(INPUT,OUTPUT,TAPE5=INPUT,TAPE6=OUTPUT)
DIMENSION DELETA(350),FTAB(100),FI(350),FA(350),FA2(350),
1VA(350),GTAB(100),G1(350),G2(350),THETA1(350),THETA2(350),
2THETAA(350),RHOTAB(100),RHOERO1(350),RHOEROA(350),ZETATAB(100),
3ZETA(350),XMBARI(350),XMCIRC1(350),XMSTAR1(350),XMPRIM1(350),
4PHIR(350),XMBARA2(350),XMCIRA2(350),XMSTRA2(350),XMPRMA2(350),
5CAPG(350),SMLG(350),ETATAB(100),DUDXTAB(75),DZDXTAB(75),
6         XMBAR2(350),XMCIRC2(350),XMSTAR2(350),XMPRIM2(350),
7XMBARA(350),XMCIRCA(350),XMSTARA(350),XMPRIMA(350),SUMRER(350),
8F2(350),XLPR(30),VWTAB(75),RMUTAB(75),ABTAB(20),FCFTAB(20),
9XMMEG(350),XMMEF(350),RRUUER(75),XL(75),XITAB(75),
1ETA(350),UEDSTAB(75),RTAB(75),RERSTAB(75),YL(100),ZETWTAB(75)
 COMMON/EPSDMU/EPSDMU(350)
 COMMON/TABLE1/RHOERO2(350)
 COMMON/TABLE2/YDL(350),RHORHOE(350)
 COMMON/THREE/NUMETA,NMAXF
 COMMON/FEB12/VWA
 COMMON/FEB11/PRTTAB(20),YDDPRT(20),NYP
 COMMON/HDCAPHE/HDCAPHE(350),GEE2
 COMMON/MUUSE/IUSEEMU,MPWEMU
 COMMON/DEC18/YCDL
 COMMON/AGAIN/TDL
 COMMON/DEC22/YS1DL,YS2DL
 COMMON/JAN7/X0
 COMMON/MAY11/A1,A2
 COMMON/JUNE1/SM,SNT
 COMMON/JULY2/YDELO
 COMMON/HIS/HIS
 COMMON/IFTC/IFTC
 COMMON/CCW/CCW
 COMMON/ZETW/ZETWTAB
 COMMON/ZETAW2/ZETAW2
 COMMON/FBAR/FBARTAB(20),IFBLU,YDDFB(20),NFBY
 COMMON/IWLDMP/IWLDMP
 NAMELIST/NAM1/NUMETA,NMAXF,NMAXG,DELETA,XK,XI0,DELXI0,XITEST,
1XISTOP,FTAB,ETATAB,VWTAB,EPSLONE,EPSLONW,         GTAB,UEDSTAB,
2 WEDS2HE,PR,ZETWTAB,XNBAR,RERSTAB,CAPRS,RTAB,J,RHOTAB,
3SHE,ZETATAB,         HSHE,XL,NUMX,YL,NUMY,    ←——————————— Removed ITHETA from NAMELIST
4X0,OL,DUDXTAB,DZDXTAB,FRO,NSTEPS,
5AP,BP,CP,ABTAB,FCFTAB,NFCFAB,PRTTAB,YDDPRT,NYP,
6XLPR,IVEG,INIT,IUSEEMU,MPWEMU,YCDL,TDL,A1,A2,SM,SNT,YDELO,
7FBARTAB,IFBLU,YDDFB,NFBY,IWLDMP
 ZETWTAB(2)=0.0
 ZETATAB(2)=0.0
```

```
            RHOTAB(2)=0.0
            ETATAB(2)=0.0
            XLPR(2)=0.0
            XIO=0.0
            NPRINT=1
            ICOUNT=1
            IFTC=0
            READ(5,NAM1)
            WRITE(6,NAM1)
     C
     C        OPTION FOR INITIAL DELTA XI
     C
            IF(INIT.EQ.0)DELXI=DELXIO
            IF(INIT.EQ.1)DELXI=XIO*1.E-5
            GEE2=1.
     C
     C        T R A N S F O R M   X   T O   X I
     C
            HRDCPHE=1.-UEDSTAB(1)**2-WEDS2HE**2
            RMUTAB(1)=SQRT(HRDCPHE/HSHE)*(HSHE+SHE)/(HRDCPHE+SHE)
           1*RERSTAB(1)*HRDCPHE
           2/HSHE
            FUNCX1=RMUTAB(1)*UEDSTAB(1)*RTAB(1)**(2*J)
            X1=XO
            DO 22 I=1,NUMX
            IF(I.EQ.1)GO TO 15
            HRDCPHE=1.-UEDSTAB(I)**2-WEDS2HE**2
            RMUTAB(I)=SQRT(HRDCPHE/HSHE)*(HSHE+SHE)/(HRDCPHE+SHE)
           1*RERSTAB(I)*HRDCPHE
           2/HSHE
            FUNCX2=RMUTAB(I)*UEDSTAB(I)*RTAB(I)**(2*J)
            SUMFXI=SUMFXI+(FUNCX2+FUNCX1)/2.*(XL(I)-XL(I-1))
            FUNCX1=FUNCX2
            GO TO 95
     15     SUMFXI=0.
     95     RRUUER(I)=CAPRS*RMUTAB(I)*UEDSTAB(I)*RTAB(I)**(2*J)
            IF(XIO.EQ.0.)GO TO 25
            GO TO 31
     25     XIO=RRUUER(I)*XI
     31     XITAB(I)=XIO+CAPRS*SUMFXI
            DUDXTAB(I)=DUDXTAB(I)/RRUUER(I)
            IF(ZETWTAB(2).NE.0.)DZDXTAB(I)=DZDXTAB(I)/RRUUER(I)
     22     CONTINUE
            XI1=XIO
```

Instead of GEE2 = GTAB(2)

(3)

```
      CCW=0.
C
C     I F   N O   E T A   T A B L E ,   T R A N S F O R M   Y   T O   E T A
C
      IF(ETATAB(2).NE.0.)GO TO 26
      ZETAW1=ZETATAB(1)  ←─────────────────────────────────────── ZETAW1=ZETWTAB(1) has changed position in program
      IF(ZETWTAB(2).EQ.0.)GO TO 3  ←─────────────────────────────── Instead of  IF(ZETATAB(2).EQ.0.) GO TO 32
      DO 202 I=1,NUMY
      THETA1(I)=(ZETATAB(I)-ZETWTAB(1))/(1.-ZETWTAB(1))
  202 CONTINUE
    3 ZW=ZETATAB(1)
      IF(ZETWTAB(2).EQ.0.)ZW=0.
      DO 33 I=1,NUMY
      IF(ZETWTAB(2).NE.0.)GO TO 32
      THETA1(I)=ZETATAB(I)
   32 RHOTAB(I)=((1.-ZW)*THETA1(I)+ZW-UEDSTAB(I)**2  ←──────────── Instead of ZETWTAB(1)
     1*FTAB(I)**2-WEDS2HE    **2*GTAB(I)**2)/(1.-UEDSTAB(I)**2-WEDS2HE
     2**2)
   33 CONTINUE  ←──────────────────────────────────────────────── Removed  32 CONTINUE
      DO 34 I=1,NUMY
      RHORHOE(I)=1./RHOTAB(I)
   34 CONTINUE
      FUNCY1=RHORHOE(1)*RERSTAB(1)
      SUMFETA=0.0
      ETATAB(1)=0.0
      DO 27 I=2,NUMY
      FUNCY2=RHORHOE(I)*RERSTAB(1)
      SUMFETA=SUMFETA+(FUNCY2+FUNCY1)/2.*(YL(I)-YL(I-1))
      FUNCY1=FUNCY2
      ETATAB(I)=CAPRS*UEDSTAB(1)*RTAB(1)**J/(2*X10)**XNBAR *SUMFETA
   27 CONTINUE
   26 CONTINUE
C
C     C O N S T A N T S
C
      ZETAE=1.
      FTEST=.99999
      GTEST=.99999
      THTEST=.99999
      ETA(1)=0.
      SUMRER(1)=0.
C
C     C O M P U T E   D E L T A   E T A S
C
```

```
      F1(1)=FTAB(1)
      G1(1)=GTAB(1)
      IF(ZETATAB(2).NE.0.)ZETA(1)=ZETATAB(1)
      IF(RHOTAB(2).NE.0.)RHOERO1(1)=RHOTAB(1)
      M=2
      DO 10 I=2,NUMETA
      DELETA(I)=XK**(I-1)*DELETA(1)
C
C     C O M P U T E   E T A   S
C     I N T E R P O L A T E   T O   G E T   F ( E T A ) S
C
      ETA(I)=ETA(I-1)+DELETA(I-1)
      IF(F1(I-1).GT..9)M=1
      CALL FTLUP(ETA(I),F1(I),M,NUMY,ETATAB,FTAB)
      M=1
      CALL FTLUP(ETA(I),G1(I),M,NUMY,ETATAB,GTAB)
      M=2
      IF(ZETA(I-1).GT..9)M=1
      CALL FTLUP(ETA(I),ZETA(I),M,NUMY,ETATAB,ZETATAB)
      M=2
   10 CONTINUE
C
C     I N I T I A L   F ( X I 1 ) S
C
      UES2HE1=UEDSTAB(1)
      RERS1=RERSTAB(1)
      R1=RTAB(1)
      DUEDX1=DUDXTAB(1)
      IF(ZETWTAB(2).NE.0)DZWDX1=DZDXTAB(1)
      CAPU1=DUEDX1/UES2HE1
      CAPP1=-CAPU1
      IF(ZETWTAB(2).NE.0)CAPZ1=DZWDX1/(1.-ZETAW1)
      XXL1=XL(1)
C
C     C O M P U T E   I N I T I A L   T H E T A S
C
      IF(ZETWTAB(2).NE.0.)GO TO 11
      DO 13 I=1,NUMETA
   13 THETA1(I)=ZETA(I)
      GO TO 12
   11 DO 201 I=1,NUMETA
      THETA1(I)=(ZETA(I)-ZETAW1)/(1.-ZETAW1)
  201 CONTINUE
   12 CONTINUE
```

Removed
```
      M=2
      IF(GTAB(2).EQ.0.)GO TO 17
```
Instead of IF(G1(I-1).GT..9)M=1

Removed
```
      GO TO 16
   17 G1(1) = 0.0
   16 IF(ZETATAB(2).EQ.0.) GO TO 18
```

Removed
```
      GO TO 19
   18 IF(ABS(RHOERO1(I-1)-1.).GE..1)M=1
      CALL FTLUP(ETA(I),RHOERO1(I),M,NUMY,ETATAB,RHOTAB)
   19 CONTINUE
```

ZETAW1=ZETWTAB(1) has changed position in program

Instead of
```
      IF(ITHETA.EQ.2)GO TO 11
      THETA1(1)=0.0
      DO 200 I=2,NUMETA
      THETA1(I)=(RHOERO1 (I)*(1.-UES2HE1**2-WEDS2HE**2)-ZETAW1+UES2HE1
     1**2*F1(I)**2+WEDS2HE**2*G1(I)**2)/(1.-ZETAW1)
  200 CONTINUE
```

(3)

(3)

41

```
C
C      IF ZETAS ARE GIVEN, INITIAL RHOERO1 S MUST
C      BE CALCULATED
C
C
       ZW=ZETAW1
       IF(ZETWTAB(2).EQ.0.)ZW=0.                              <——————————— Removed IF(ZETATAB(2).EQ.0.) GO TO 28
       DO 29 I=1,NUMETA
       RHOERO1(I)=((1.-ZW)*THETA1(I)+ZW-UES2HE1**2*F1(I)**2    <——————————— Instead of ZETAW1
      1-WEDS2HE**2*G1(I)**2)/(1.-UES2HE1**2-WEDS2HE**2)
    29 CONTINUE                                               ————————————— Removed 28  CONTINUE
       DO 21 I=1,NUMETA
       RHORHOE(I)=1./RHOERO1(I)
    21 RHOERO2(I)=RHOERO1(I)
C
C      COMPUTE INITIAL VS
C
       XIBAR1=(2.*XI0)**(2.*XNBAR )
       VA(1)=(2*XI1)**XNBAR /R1**J*RHORHOE(1)*RERS1*VWTAB(1)/RMUTAB(1)  ———— Removed IF(GEE2.NE.0.)VA(1)=VA(1)*WEDS2HE/UES2HE1
       DO 20 I=2,NUMETA
       VA(I)=VA(I-1)-DELETA(I-1)*XIBAR1*(F1(I)+F1(I-1))*XNBAR /(2.*XI0)
    20 CONTINUE
       YDL(1)=0.0
       FNCRER1=RHOERO2(1)
       DO 42 I=2,NUMETA
       FNCRER2=RHOERO2(I)
       SUMRER(I)=SUMRER(I-1)+(FNCRER2+FNCRER1)/2.*DELETA(I-1)
       FNCRER1=FNCRER2
       YDL (I)=(2.*XI1)**XNBAR *1./RERS1*SUMRER(I)/(CAPRS*R1**J*UES2HE1)
    42 CONTINUE
C
C      CALCULATE INITIAL MS
C
       VWA=VWTAB(1)                                           ————————————— Removed IF(GEE2.NE.0.)VWA=VWA*WEDS2HE/UES2HE1
       DO 44 I=1,NUMETA
       HDCAPHE(I)=(1.-ZW)*THETA1(I)+ZW-UES2HE1**2*F1(I)**2    <——————————— Instead of ZETAW1
      1-WEDS2HE**2*G1(I)**2
    44 CONTINUE
       CALL CALCM(ZETAW1,UES2HE1,F1,WEDS2HE,ZETAE,
      1              SHE,PR,    XMBAR1,XMCIRC1,XMSTAR1,XMPRIM1,PHIR,
      2HSHE,        RERS1,XI1,XNBAR ,R1,J,
      3DELETA,RURDRUS,   CAPRS,SUMRER,AP,BP,CP,       ABTAB,FCFTAB,NFCFAB,
      4NMAXG,G1,XXL1)
    40 CONTINUE
C
```

```
C     B E G I N   N E W   I N T E R V A L
C
      IF(XI1.GE.XI0+30.*DELXI.AND.INIT.EQ.1)GO TO 46
      GO TO 48
   46 DELXI=DELXI0
      INIT=0
   48 CONTINUE
      IF(XI1.LT.XITEST)GO TO 35
      DELXI=DELXI*10.
      XITEST=XITEST*10.
   35 XI2=XI1+DELXI
      IF(ICOUNT.EQ.1)XI2=XI1
      XIA=(XI1+XI2)/2.
      ITERATE=1
      DO 30 I=1,NUMETA
      F2(I)=F1(I)
      FA(I)=F1(I)
      G2(I)=G1(I)
      THETA2(I)=THETA1(I)
      THETAA(I)=THETA1(I)
      XMBAR2(I)=XMBAR1(I)
   30 CONTINUE
   52 CONTINUE
C
C     I N T E R P O L A T E   F O R   F ( X I 2 ) S
C
      CALL FTLUP(XI2,XXL2,1,NUMX,XITAB,XL)
      CALL FTLUP(XIA,RA,1,NUMX,XITAB,RTAB)
      CALL FTLUP(XIA,RERSA,1,NUMX,XITAB,RERSTAB)
      CALL FTLUP(XIA,RMRRMSA,1,NUMX,XITAB,RMUTAB)
      CALL FTLUP(XIA,VWA,1,NUMX,XITAB,VWTAB)
      CALL FTLUP(XIA,RRUUERA,1,NUMX,XITAB,RRUUER)
      CALL FTLUP(XI2,UES2HF2,1,NUMX,XITAB,UEDSTAB)
      CALL FTLUP(XI2,RERS2,1,NUMX,XITAB,RERSTAB)
      CALL FTLUP(XI2,R2,1,NUMX,XITAB,RTAB)
      CALL FTLUP(XI2,DUEDX2,1,NUMX,XITAB,DUDXTAB)
      IF(ZETWTAB(2).EQ.0.)GO TO 203
      CALL FTLUP(XI2,ZETAW2,1,NUMX,XITAB,ZETWTAB)    ← ——— Changed position
      CALL FTLUP(XI2,DZWDX2,1,NUMX,XITAB,DZDXTAB)
      CAPZ2=DZWDX2/(1.-ZETAW2)    ← ——— Changed position
  203 CONTINUE
      UES2HEA=(UES2HE1+UES2HE2)/2.
      CAPU2=DUEDX2/UES2HE2
      CAPP2=-CAPU2
```

③

43
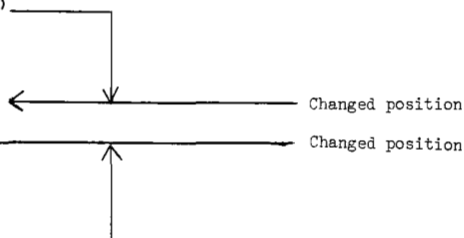
```
      XIBAR2=(2.*XI2)**(2.*XNBAR)
      XIBARA=(XIBAR1+XIBAR2)/2.
      XIBCPUA=(XIBAR1*CAPU1+XIBAR2*CAPU2)/2.
      XIBCPPA=(XIBAR1*CAPP1+XIBAR2*CAPP2)/2.
      IF(ZETWTAB(2).NE.O.)XIBCPZA=(XIBAR1*CAPZ1+XIBAR2*CAPZ2)/2.
      IF(ICOUNT.EQ.1)GO TO 110                    ←———————————————  Removed  IF(GEE2.NE.O.)VWA=VWA*WEDS2HE/UES2HEA
C
C     I T E R A T E   W I T H   S A M E   X I 2
C
   37 CONTINUE
      ZW=ZETAW2
      IF(ZETWTAB(2).EQ.0.)ZW=0.                    ———————————————  Removed  37
      DO 36 I=1.NUMETA                                              Instead of ZETAW2
      RHOERO2(I)=((1.-ZW)*THETA2(I)+ZW-UES2HE2**2*F2(I)**2  ←——————
     1-WEDS2HE**2*G2(I)**2)/(1.-UES2HE2**2-WEDS2HE**2)
      RHOEROA(I)=(RHOERO1(I)+RHOERO2(I))/2.
      RHORHOE(I)=1./RHOERO2(I)
   36 CONTINUE
      FNCRER1=RHOERO2(1)
      DO 38 I=2.NUMETA
      FNCRER2=RHOERO2(I)
      SUMRER(I)=SUMRER(I-1)+(FNCRER2+FNCRER1)/2.*DELETA(I-1)
      FNCRER1=FNCRER2
      YDL (I)=(2.*XI2)**XNBAR *1./RERS2*SUMRER(I)/(CAPRS*R2**J*UES2HE2)
   38 CONTINUE
C
C     C A L C U L A T E   M S
C
      DO 39 I=1.NUMETA
      HDCAPHE(I)=(1.-ZW)*THETA2(I)+ZW-UES2HE2**2*F2(I)**2   ←———————  Instead of ZETAW2
     1-WEDS2HE**2*G2(I)**2
   39 CONTINUE
      CALL CALCM(ZETAW2.UES2HE2.F2.WEDS2HE.ZETAE.
     1              SHE.PR.    XMBAR2.XMCIRC2.XMSTAR2.XMPRIM2.PHIR.
     2HSHE.        RERS2.XI2.XNBAR .R2.J.
     3DELETA.RURDRUS.   CAPRS.SUMRER.AP.BP.CP.    ABTAB.FCFTAB.NFCFAB.
     4NMAXG.G2.XXL2)
      DO 54 I=1.NUMETA
      XMBARA(I)=(XMBAR1(I)+XMBAR2(I))/2.
      IF(GEE2.NE.O.)XMCIRCA(I)=(XMCIRC1(I)+XMCIRC2(I))/2.
      XMSTARA(I)=(XMSTAR1(I)+XMSTAR2(I))/2.
      XMPRIMA(I)=(XMPRIM1(I)+XMPRIM2(I))/2.
   54 CONTINUE
      NUMDELE=NUMETA-1
```

③ (annotation markers at left margin near lines 37/ZW=ZETAW2/IF(ZETWTAB), RHOERO2, and HDCAPHE)

```
      DO 50 I=1,NUMDELE
      XMBARA2(I)=(XMBARA(I+1)+XMBARA(I))/2.
      IF(GEE2.NE.0.)XMCIRA2(I)=(XMCIRCA(I+1)+XMCIRCA(I))/2.
      XMSTRA2(I)=(XMSTARA(I+1)+XMSTARA(I))/2.
      XMPRMA2(I)=(XMPRIMA(I+1)+XMPRIMA(I))/2.
   50 CONTINUE
C
C     C A L C U L A T E   F S
C
      ICHD=1
      FPREV=F2(2)
   55 CALL ABCDGS(NUMDELE,DELETA,XIBARA,DELXI,FA,VA,XMBARA2,ICHD,F1,
     1XIBCPUA,XIBCPPA,RHOEROA,G1,THETA1,XIBCPZA,THETAA,UES2HEA,XMPRMA2,
     2F2,WEDS2HE,G2,CAPG,SMLG,XK)
      CALL COMPUTE(NMAXF,FTEST,NUMDELE,DELETA,EPSLONE,CAPG,SMLG,ICHD,F2)
C
C     U P D A T E   F A S   A N D   V A S
C
      DO 70 I=2,NUMETA
      FA(I)=(F1(I)+F2(I))/2.
   70 CONTINUE
      DO 73 I=1,NUMDELE
      FA2(I)=(FA(I+1)+FA(I))/2.
   73 CONTINUE
      TIMES=XNBAR/XIA
      VA(1)=(2*XIA)**XNBAR /RA**J/RHOEROA(1)*RERSA*VWA/RMRRMSA
      DO 74 I=2,NUMETA
      VA(I)=VA(I-1)-DELETA(I-1)*XIBARA/(2.*DELXI)*(F2(I)+F2(I-1)-F1(I)
     1-F1(I-1))-DELETA(I-1)*XIBARA*FA2(I-1)*TIMES
   74 CONTINUE
C
C     C A L C U L A T E   G S
C
      IF(GEE2.EQ.0.)GO TO 75
      ICHD=2
      GPREV=G2(2)
      CALL ABCDGS(NUMDELE,DELETA,XIBARA,DELXI,FA,VA,XMCIRA2,ICHD,F1,
     1XIBCPUA,XIBCPPA,RHOEROA,G1,THETA1,XIBCPZA,THETAA,UES2HEA,XMPRMA2,
     2F2,WEDS2HE,G2,CAPG,SMLG,XK)
      CALL COMPUTE(NMAXG,GTEST,NUMDELE,DELETA,EPSLONE,CAPG,SMLG,ICHD,G2)
C
C     C A L C U L A T E   T H E T A S
C
   75 CONTINUE
```

③

③

— Instead of IF(GTAB(2).EQ.0.)GO TO 75

```
      ICHD=3
      THETAPR=THETA2(2)
      CALL ABCDGS(NUMDELE,DELETA,XIBARA,DELXI,FA,VA,XMSTRA2,ICHD,F1,
     1XIBCPUA,XIBCPPA,RHOEROA,G1,THETA1,XIBCPZA,THETAA,UES2HEA,XMPRMA2,
     2F2,WEDS2HE,G2,CAPG,SMLG,XK)
      IF(XI1.EQ.XIO.AND.ITERATE.EQ.1)NMAXTH=1.1*NMAXF
      CALL COMPUTE(NMAXTH,THTEST,NUMDELE,  DELETA,EPSLONE,CAPG,SMLG,
     1ICHD,THETA2)
C
C     U P D A T E   T H E T A S
C
      DO 76 I=1,NUMETA
   76 THETAA(I)=(THETA1(I)+THETA2(I))/2.
      ITERATE=ITERATE+1
      IF(ITERATE.EQ.2)GO TO 37
C
C     C O N V E R G E N C E   C R I T E R I A
C
C
      IF(ABS((F2(2)-FPREV)/FPREV).LE.EPSLONW)GO TO 90
      GO TO 37
   90 IF(GEE2.EQ.0.)GO TO 100
      IF(ABS((G2(2)-GPREV)/GPREV).LE.EPSLONW)GO TO 100
      GO TO 37
  100 IF(ABS((THETA2(2)-THETAPR)/THETAPR).LE.EPSLONW)GO TO 110
      GO TO 37
  110 CONTINUE
C     O U T P U T
C
C
C
C     C O M P U T E   RHOERHO S
C
      DO 80 I=1,NUMETA
      RHOERO2(I)=((1.-ZW)*THETA2(I)+ZW-UES2HE2**2*F2(I)**2-
     1WEDS2HE**2*G2(I)**2)/(1.-UES2HE2**2-WEDS2HE**2)
      RHORHOE(I)=1./RHOERO2(I)
      XMMEF(I)=F2(I)*SQRT(RHORHOE(I))
   80 CONTINUE
      FNCRER1=RHOERO2(1)
      DO 102 I=2,NUMETA
      FNCRER2=RHOERO2(I)
      SUMRER(I)=SUMRER(I-1)+(FNCRER2+FNCRER1)/2.*DELETA(I-1)
      FNCRER1=FNCRER2
      YDL (I)=(2.*XI2)**XNBAR *1./RERS2*SUMRER(I)/(CAPRS*R2**J*UES2HE2)
```

Instead of ZETAW2

Removed IF(GEE2.NE.0.)XMMEG(I)=G2(I)*SQRT(RHORHOE(I))

③ ③

```
    102 CONTINUE                                              ←————————————————————————————————— Removed CALL FTLUP(XI2,XXL,1,NUMX,XITAB,XL)
        IF(XLPR(2).EQ.0.)GO TO 116
        IF(XXL2.GE.XLPR(NPRINT))GO TO 103
        IF(ICOUNT.EQ.1)GO TO 103

        GO TO 115
    116 IF(NPRINT.EQ.NSTEPS)GO TO 101
        NPRINT=NPRINT+1
        IF(ICOUNT.EQ.1)GO TO 103
        GO TO 115
    101 NPRINT=1
    103 CONTINUE
        DO 91 I=1,NUMETA
        ZETA(I)=THETA2(I)*(1.-ZW)+ZW                          ←————————————————————————————————— Instead of ZETAW2
     91 CONTINUE
        WRITE(6,111)XI2,XXL2
    111 FORMAT(1H0,3HXI=,E20.8,4X,4HX/L=,E20.8)
        MAX=NMAXF+10
        GO TO (117,118,119)IVEG
    117 WRITE(6,112)
    112 FORMAT(1H0,7X,3HETA,11X,3HY/L,12X,1HF,13X,1HV,11X,5HTHETA,9X,
       14HZETA,8X,8HRHO/RHOE,8X,5HM/MEF)
        DO 113 I=1,MAX
        WRITE(6,114)I,ETA(I),YDL(I),F2(I),VA(I),THETA2(I),ZETA(I),
       1RHORHOE(I),XMMEF(I)
    113 CONTINUE
        GO TO 115
    114 FORMAT(I4,9E14.4)
    118 WRITE(6,141)
    141 FORMAT(1H0,7X,3HETA,11X,3HY/L,12X,1HF,11X,6HEPSDMU,8X,5HTHETA,
       19X,4HZETA,8X,8HRHO/RHOE,8X,5HM/MEF)
        DO 142 I=1,MAX
        WRITE(6,114)I,ETA(I),YDL (I),F2(I),EPSDMU(I),THETA2(I),ZETA(I),
       1RHORHOE(I),XMMEF(I)
    142 CONTINUE
        GO TO 115
    119 WRITE(6,143)
    143 FORMAT(1H0,7X,3HETA,11X,3HY/L,12X,1HF,13X,1HG,11X,5HTHETA,9X,
       14HZETA,8X,8HRHO/RHOE,8X,5HXMBAR,11X,5HXMMEF)
        DO 144 I=1,MAX
        WRITE(6,114)I,ETA(I),YDL (I),F2(I),G2(I),THETA2(I),ZETA(I),
       1RHORHOE(I),XMBAR2(I),XMMEF(I)
    144 CONTINUE
    115 CONTINUE
      C
```

③

```
C     U P D A T E   V A L U E S
C
      XIBAR2=(2.*XI2)**(2.*XNBAR)
      DO 120 I=1,NUMETA
      F1(I)=F2(I)
      G1(I)=G2(I)
      THETA1(I)=THETA2(I)
      RHOERO1(I)=RHOERO2(I)
  120 CONTINUE
      UES2HE1=UES2HE2
      ZETAW1=ZETAW2
      DO 106 I=1,NUMETA
      HDCAPHE(I)=(1.-ZW)*THETA1(I)+ZW-UES2HE1**2*F1(I)**2          <──────────────── Instead of ZETAW2
     1-WEDS2HE**2*G1(I)**2
  106 CONTINUE
      CALL CALCM(ZETAW2,         UES2HE1,F1,WEDS2HE,          ZETAE,
     1               SHE,PR,    XMBAR1,XMCIRC1,XMSTAR1,XMPRIM1,PHIR,
     2HSHE,          RERS2,XI2,XNBAR ,R2,J,
     3DELETA,RURDRUS,     CAPRS,SUMRER,AP,BP,CP,       ABTAB,FCFTAB,NFCFAB,
     4NMAXG,G1,XXL2)
      IF(ICOUNT.EQ.1)GO TO 104
      IF(XLPR(2).EQ.0.)GO TO 145
      IF(XXL2.GE.XLPR(NPRINT))GO TO 105
      GO TO 123
  105 NPRINT=NPRINT+1
      GO TO 104
  145 IF(NPRINT.NE.1)GO TO 123
  104 CONTINUE
      XINB=(2.*XI2)**XNBAR
      CFF=PHIR(1)/RERS2*2.*R2**J/XINB*(F2(2)-F2(1))/DELETA(1)*RURDRUS    ────── Removed IF(GEE2.NE.0.)CFG=PHIR(1)/RERS2*2.*R2**J/XINB*(G2(2)-G2(1))/
      SUMF=0.0   <─────                                                         DELETA(1)*UES2HE1/WEDS2HE*RURDRUS
      FUNCF1=F2(1)*(1.-F2(1))                                                   IF(GEE2.NE.0.)ZETDIAG=CFF/CFG*(UES2HE1/WEDS2HE)**2
      DO 92 I=2,NMAXF
      FUNCF2=F2(I)*(1.-F2(I))
      SUMF=SUMF+(FUNCF2+FUNCF1)/2.*(ETA(I)-ETA(I-1))
      FUNCF1=FUNCF2
   92 CONTINUE
      RCURJ=RERS2*CAPRS*UES2HE2*R2**J
      TSDLF=XINB/RCURJ*SUMF
      GO TO 150   <──────────────────────────────────────────────────────── Instead of IF(GEE2.EQ.0.)GO TO 150
      SUMG=0.0
      FUNCG1=G2(1)*(1.-G2(1))
      DO 94 I=2,NMAXG
      FUNCG2=G2(I)*(1.-G2(I))
```

```
      SUMG=SUMG+(FUNCG2+FUNCG1)/2.*(ETA(I)-ETA(I-1))
      FUNCG1=FUNCG2
   94 CONTINUE
      TSDLG=XINB/RCURJ*SUMG
  150 CONTINUE
      SMDEL=0.0
      SMTHF=0.0
      FNCDEL1=1.-F2(1)
      FNCTHE1=F2(1)*(1.-F2(1))
      DO 56 I=2,NMAXF
      FNCDEL2=1.-F2(I)
      FNCTHE2=F2(I)*(1.-F2(I))
      SMDEL=SMDEL+(FNCDEL2+FNCDEL1)/2.*(YDL(I)-YDL(I-1))
      SMTHE=SMTHE+(FNCTHE2+FNCTHE1)/2.*(YDL(I)-YDL(I-1))
      FNCDEL1=FNCDEL2
      FNCTHE1=FNCTHE2
   56 CONTINUE            <———————————————————————————— Removed HISF=SMDEL/SMTHE
      GO TO 151           <———————————————————————————— Instead of IF(GEE2.EQ.0.)GO TO 151
      SMDEL=0.0
      SMTHE=0.0
      FNCDEL1=1.-G2(1)
      FNCTHE1=G2(1)*(1.-G2(1))
      DO 57 I=2,NMAXG
      FNCDEL2=1.-G2(I)
      FNCTHE2=G2(1)*(1.-G2(I))
      SMDEL=SMDEL+(FNCDEL2+FNCDEL1)/2.*(YDL (I)-YDL (I-1))
      SMTHE=SMTHE+(FNCTHE2+FNCTHE1)/2.*(YDL (I)-YDL (I-1))
      FNCDEL1=FNCDEL2
      FNCTHE1=FNCTHE2
   57 CONTINUE
      HISG=SMDEL/SMTHE
  151 CONTINUE
      SUMFRR=0.0
      FNCFRR1=1.-F2(1)*RHORHOE(1)
      DO 93 I=2,NMAXF
      FNCFRR2=1.-F2(I)*RHORHOE(I)
      SUMFRR=SUMFRR+(FNCFRR2+FNCFRR1)/2.*(YDL(I)-YDL(I-1))
      FNCFRR1=FNCFRR2
   93 CONTINUE
      DSDLF=SUMFRR
      GO TO 96            <———————————————————————————— Instead of IF(GEE2.EQ.0.)GO TO 96
      SUMGRR=0.0
      FNCGRR1=1.-G2(1)*RHORHOE(1)
      DO 97 I=2,NMAXG
```

```
      FNCGRR2=1.-G2(I)*RHORHOE(I)
      SUMGRR=SUMGRR+(FNCGRR2+FNCGRR1)/2.*(YDL (I)-YDL (I-1))
      FNCGRR1=FNCGRR2
   97 CONTINUE
      DSDLG=SUMGRR
   96 CONTINUE
      REX=CAPRS*XXL2*UES2HF2*RERS2**2/RURDRUS
      RDXL=REX/XXL2
      RETSF=RDXL*TSDLF
      REDSF=RDXL*DSDLF
      HFDCPHE=1.-UES2HE2**2-WEDS2HE**2
      QBAR=PHIR(1)*RURDRUS*R2**J*UES2HE2*CAPRS/(PR*XINB)*(ZETA(2)
     1       -ZETA(1))/DELFTA(1)
      ST=QBAR/(RERS2*CAPRS*UES2HE2*(FRO*(1.-HEDCPHE)+HEDCPHE-ZETA(1)))
      WRITE(6,121)
  121 FORMAT(1H0,7X,3HCFF,10X,9HTHETA*/LF,7X,9HDELTA*/LF,9X,3HREX,11X,
     19HRETHETA*F,7X,9HREDFLTA*F,9X,4HQBAR,13X,2HST)
      WRITE(6,122)CFF,TSDLF,DSDLF,REX,RETSF,REDSF,QBAR,ST
  122 FORMAT(8E16.4)
      WRITE(6,124)
  124 FORMAT(1H0,7X,4HHI*F,11X,3HCCW)
      WRITE(6,122)HIS,CCW
      GO TO 98
      WRITE(6,131)
  131 FORMAT(1H0,7X,3HCFG,10X,9HTAUF/TAUG,6X,9HTHETA*/LG,7X,
     19HDELTA*/LG,7X,9HRETHETA*G,7X,9HREDELTA*G,9X,4HHI*G)
      WRITE(6,122)CFG,TAFDTAG,TSDLG,DSDLG,RETSG,REDSG,HISG
   98 CONTINUE
      WRITE(6,132)
  132 FORMAT(1H0,5X,5HYS1DL,11X,5HYS2DL)
      WRITE(6,122)YS1DL,YS2DL
      ICOUNT=ICOUNT+1
  123 CONTINUE
      IF(XISTOP.LE.XI2)GO TO 130
      XI1=XI2
      XI8AR1=XI8AR2
      CAPU1=CAPU2
      CAPP1=CAPP2
      IF(ZETWTAB(2).NE.0.)CAPZ1=CAPZ2
      XXL1=XXL2
      GO TO 40
  130 CONTINUE
      STOP
      END
```

Removed  IF(G.....0.)RETSG=RDXI*TSDLG*WEDS2HE/UES2HE

Removed  IF(G.......0.) G.XG=RDXL*DSDLG*.....L/UES.....

(1)

Instead of IF(GEE2.EQ.0.)GO TO 98

(1) {

(3) {

```
      SUBROUTINE ABCDGS(NUMDELE,DELETA,XIBARA,DELXI,FA,VA,CAPMA2,ICHD,
     1F1,XIBCPUA,XIBCPPA,RHOEROA,G1,THETA1,XIBCPZA,THETAA,UES2HEA,
     2XMPRMA2,F2,WEDS2HE,G2,CAPG,SMLG,XK)
      DIMENSION DELETA(350),F1(350),F2(350),FA(350),G1(350),G2(350),
     1THETA1(350),THETA2(350),THETAA(350),VA(350),CAPMA2(350),CAPA(350),
     2CAPB(350),CAPC(350),CAPD(350),RHOEROA(350),XMPRMA2(350),CAPG(350),
     3SMLG(350),ZETWTAB(75)
      COMMON/ZETW/ZETWTAB
      FCT1=2.*XK/(1.+XK)
      FCT2=2./(1.+XK)
      DO 10 I=2,NUMDELE
      DELDEL2=2.*DELETA(I)*DELETA(I-1)
      XIDELFA=XIBARA/DELXI*FA(I)
      VADLDL2=VA(I)/(2.*(DELETA(I)+DELETA(I-1)))
      TMDLDL2=(CAPMA2(I)*FCT2+CAPMA2(I-1)*FCT1)/DELDEL2
      CAPA(I)=VADLDL2-CAPMA2(I)*FCT2/DELDEL2
      CAPB(I)=XIDELFA+TMDLDL2
      CAPC(I)=-(VADLDL2+CAPMA2(I-1)*FCT1/DELDEL2)
      IF(ICHD.EQ.1)GO TO 20
      IF(ICHD.EQ.2)GO TO 30
      IF(ICHD.EQ.3)GO TO 40
   20 CAPD(I)=-CAPA(I)*F1(I+1)+(XIDELFA-TMDLDL2)*F1(I)-CAPC(I)*F1(I-1)
     1-XIBCPUA*FA(I)**2-XIBCPPA*RHOEROA(I)
      GO TO 10
   30 CAPD(I)=-CAPA(I)*G1(I+1)+(XIDELFA-TMDLDL2)*G1(I)-CAPC(I)*G1(I-1)
      GO TO 10
   40 CAPD(I)=-CAPA(I)*THETA1(I+1)+(XIDELFA-TMDLDL2)*THETA1(I)-CAPC(I)*
     1THETA1(I-1)-UES2HEA**2/DELDEL2*
     2(XMPRMA2(I)*FCT2*(F1(I+1)**2+F2(I+1)**2-F1(I)**2-F2(I)**2)
     3-XMPRMA2(I-1)*FCT1*(F1(I)**2+F2(I)**2-F1(I-1)**2-F2(I-1)**2))
     4-WEDS2HE**2/DELDEL2*(XMPRMA2(I)*FCT2*(G1(I+1)**2+G2(I+1)**2
     5-G1(I)**2-G2(I)**2)-XMPRMA2(I-1)*FCT1*(G1(I)**2+G2(I)**2-G1(I-1)
     6**2-G2(I-1)**2))
      IF(ZETWTAB(2).NE.0.)CAPD(I)=CAPD(I)+XIBCPZA*FA(I)*(THETAA(I)-1.)
   10 CONTINUE
      IF(ZETWTAB(2).NE.0..AND.ICHD.EQ.2)GO TO 41
      IF(ZETWTAB(2).EQ.0..AND.ICHD.NE.1)GO TO 41
      CAPG(2)=-CAPA(2)/CAPB(2)
      SMLG(2)=CAPD(2)/CAPB(2)
      GO TO 42
   41 CAPG(2)=-CAPA(2)/(CAPB(2)+CAPC(2))
      SMLG(2)=CAPD(2)/(CAPB(2)+CAPC(2))
   42 CONTINUE
      DO 50 I=3,NUMDELE
      BCG=CAPB(I)+CAPC(I)*CAPG(I-1)
      CAPG(I)=-CAPA(I)/BCG
      SMLG(I)=(CAPD(I)-CAPC(I)*SMLG(I-1))/BCG
   50 CONTINUE
      RETURN
      END
```

③ (circled, left margin near COMMON line)

③ (circled, left margin near statement 40)

removed +XIBCPZA*FA(I)*(THETAA(I)-1.)  (handwritten annotation to right of statement 40)

② (circled, left margin near IF(ZETWTAB(2)... lines)

() (circled, left margin near 41)

```
      SUBROUTINE CALCM(ZETAW,UEDS2HE,F2,WEDS2HE,ZETAE,
     1             SHE,PR,   XMBAR,XMCIRC,XMSTAR,XMPRIM,PHIR,HSHE,
     2        RERS,XI,XNBAR,R,J,                           DELETA,
     3RURDRUS,    CAPRS,SUMRER,AP,BP,CP,   ABTAB,FCFTAB,NFCFAB,NMAXG,
     4G2,XXL)
       DIMENSION F2(350),G2(350),XMBAR(350),XMCIRC(350),
      1XMSTAR(350),XMPRIM(350),PHIR(350),DELETA(350),SUMRER(350),
      2ABTAB(20),FCFTAB(20),EMUSDMU(350),ZETWTAB(75)
       COMMON/EPSDMU/EPSDMU(350)
       COMMON/TABLE1/RHOERO2(350)
       COMMON/TABLE2/YDL(350),RHORHOE(350)
       COMMON/THREE/NUMETA,NMAXF
       COMMON/FEB12/VWA
       COMMON/FEB11/PRTTAB(20),YDDPRT(20),NYP
       COMMON/HDCAPHE/HDCAPHE(350),GEE2
       COMMON/MUUSE/IUSEEMU,MPWEMU
       COMMON/DEC18/YCDL
       COMMON/AGAIN/TDL
       COMMON/DEC22/YS1DL,YS2DL
       COMMON/JAN7/X0
       COMMON/MAY11/A1,A2
       COMMON/JUNE1/SM,SNT
       COMMON/JULY2/YDELO
       COMMON/HIS/HIS
       COMMON/IFTC/IFTC
       COMMON/CCW/CCW
       COMMON/ZETW/ZETWTAB
       COMMON/FBAR/FBARTAB(20),IFBLU,YDDFB(20),NFBY
       COMMON/IWLDMP/IWLDMP
       HRDCPHE=ZETAE-UEDS2HE**2-WEDS2HE**2
       RURDRUS=SQRT(HRDCPHE/HSHE)*(HSHE+SHE)/(HRDCPHE+SHE)
      1*RERS*HRDCPHE
      2/HSHE
       RUSDRUR=1./RURDRUS
       SMRER=0.0
       FNCRER1=RHOERO2(1)
       DO 25 I=2,NMAXF
       FNCRER2=RHOERO2(I)
       SMRER=SMRER+(FNCRER2+FNCRER1)/2.*DELETA(I-1)
       IF(F2(I).GE..995)GO TO 23
       FNCRER1=FNCRER2
   25 CONTINUE
       GO TO 23
   24 CONTINUE
```

Removed IF(GEE2.NE.0.)GO TO 24

```
      DO 22 I=2,NMAXG
      FNCRER2=RHOERO2(I)
      SMRER=SMRER+(FNCRER2+FNCRER1)/2.*DELETA(I-1)
      IF(G2(I).GE..995)GO TO 23
      FNCRER1=FNCRER2
   22 CONTINUE
   23 CONTINUE
      NDEL=I
      YDEL=YDL(NDEL)
      DO 60 I=2,NMAXG
      IF(G2(I).GE..01+.99*CCW)GO TO 61
   60 CONTINUE
   61 YS1DL=YDL(I)
      DO 70 JJ=I,NMAXG
      IF (G2(JJ).GE..5)GO TO 71
   70 CONTINUE
   71 YDLG=YDL(JJ)
      DO 62 K=JJ,NMAXG
      IF(G2(K).GE..99+.01*CCW)GO TO 63
   62 CONTINUE
   63 YS2DL=YDL(K)
      IF(YS1DL.LT.0.)YS1DL=0.
      SMDEL=0.0
      SMTHE=0.0                          ← ─────────────────────── Removed IF(GEE2.NE.0.)GO TO 26
      FNCDEL1=1.-F2(I)
      FNCTHE1=F2(I)*(1.-F2(I))
      IP1=I+1
      DO 27 I=IP1,NMAXF
      FNCDEL2=1.-F2(I)
      FNCTHE2=F2(I)*(1.-F2(I))
      SMDEL=SMDEL+(FNCDEL2+FNCDEL1)/2.*(YDL(I)-YDL(I-1))
      SMTHE=SMTHE+(FNCTHE2+FNCTHE1)/2.*(YDL(I)-YDL(I-1))
      FNCDEL1=FNCDEL2
      FNCTHE1=FNCTHE2
   27 CONTINUE
      GO TO 28
   26 CONTINUE
      FNCDEL1=1.-G2(1)
      FNCTHE1=G2(1)*(1.-G2(1))
      DO 11 I=2,NMAXG
      FNCDEL2=1.-G2(I)
      FNCTHE2=G2(I)*(1.-G2(I))
      SMDEL=SMDEL+(FNCDEL2+FNCDEL1)/2.*(YDL (I)-YDL (I-1))
      SMTHE=SMTHE+(FNCTHE2+FNCTHE1)/2.*(YDL (I)-YDL (I-1))
```

② (marginal note near lines 23–63)

② (marginal note near IP1=I+1 / DO 27)

```
      FNCDEL1=FNCDEL2
      FNCTHE1=FNCTHE2
   11 CONTINUE
   28 CONTINUE
      HIS=SMDEL/SMTHE
      A3=FBARMAX=AP+BP*HIS+CP*HIS*HIS
      IF(XXL.NE.X0)GO TO 72
      YDDO=(2.*YCDL+TDL)/YDEL0+A3/.4*(1.+(-2.*YCDL-.5*TDL)/YDELO)
   72 CONTINUE
      DO 12 I=1,NUMETA
      PHIR(I)=SQRT(HDCAPHE(I)/HRDCPHE)*(HRDCPHE+SHE)/(HDCAPHE(I)+SHE)
      EMUSDMU(I)=RUSDRUR*RHORHOE(I)*RERS/PHIR(I)
   12 CONTINUE
      DO 10 I=1,NUMETA
      YDD=SUMRER(I)/SMRER
      CALL DISCOT(YDD,YDD,YDDPRT,PRTTAB,PRTTAB,-11,NYP,0,PRT)
      IF(I.EQ.1)GO TO 32
      IF(IFBLU.EQ.1)GO TO 13
      YDLDDEL=YDL(I)/YDEL
      YS2MYS1=(YS2DL-YS1DL)*SNT
      YDLMYS1=YDEL-YS1DL
      IF(IFTC.GE.1)GO TO 52
      IF(CCW .GE..85)GO TO 52
      IF(YS2MYS1*A2/A3.GE.YDLMYS1)GO TO 52
      A1YCDL=A1*YCDL
      A2YS2M1=A2*YS2MYS1
      TWO=(.8-A1)*YCDL/.4*YDEL/YDELO
      AMADTMY=(A1YCDL-A2YS2M1)/(TWO-YDLG)
      YDDOYDL=YDDO*YDEL
      IF(YS2MYS1.LE.YCDL*A1/A2)GO TO 50
      IF(YS2MYS1.GT.YCDL*A1/A2)GO TO 51
   50 YCDLDDL=YCDL/YDEL
      ONE=A1*YCDL/.4
      IF(YDL(I).LE.ONE)FBAR=.4*YDLDDEL
      IF(ONE.LE.YDL(I).AND.YDL(I).LE.TWO)FBAR= A1*YCDLDDL
      IF(TWO.LE.YDL(I).AND.YDL(I).LE.YDLG)FBAR=YDLDDEL*AMADTMY+A1YCDL/
     1YDEL-TWO*AMADTMY/YDEL
      IF(YDLG.LE.YDL(I).AND.YDL(I).LE.YDDOYDL)FBAR=A2YS2M1/YDEL+(YDL(I)-
     1YDLG)/YDEL*(A3*(YDEL-YS1DL)-A2*YS2MYS1)/(YDDOYDL-YDLG)
      IF(YDL(I).GT.YDDOYDL)FBAR=A3*(1.-YS1DL/YDEL)
      GO TO 53
   51 ONE=A2*YS2MYS1/.4
      IF(YDL(I).LT.ONE)FBAR=.4*YDLDDEL
      IF(ONE.LE.YDL(I).AND.YDL(I).LE.YDLG)FBAR= A2*YS2MYS1/YDEL
```

```
      IF(YDLG.LE.YDL(I).AND.YDL(I).LE.YDDOYDL)FBAR=A2YS2M1/YDEL+(YDL(I)-
     1YDLG)/YDEL*(A3*(YDEL-YS1DL)-A2*YS2MYS1)/(YDDOYDL-YDLG)
      IF(YDL(I).GT.YDDOYDL)FBAR= A3*(1.-YS1DL/YDEL)
      GO TO 53
   52 IFTC=IFTC+1
 2007 IF(YDL(I).LE..1*YDEL)FBAR=.4*YDLDDEL
      IF(YDLDDEL.GT..1.AND.YDLDDEL.LE..3)FBAR=.04+(YDLDDEL-.1)/.2
     1*(FBARMAX-.04)
      IF(YDLDDEL.GT..3)FBAR=FBARMAX
   53 CONTINUE
      GO TO 14
   13 CALL DISCOT(YDD,YDD,YDDFB,FBARTAB,FBARTAB,-11,NFBY,0,FBAR)
   14 CONTINUE
      IF(I.EQ.NUMETA)GO TO 32                         ─── Removed IF(GEE2.NE.0.)GO TO 29
      EPSDMU(I)=(2.*XI)**XNBAR/R**J* FBAR**2*EMUSDMU(I)*RHORHOE(I)**2*
     1SMRER**2
     1*ABS((F2(I+1)-F2(I-1))/(DELETA(I)+DELETA(I-1)))
      GO TO 34
   29 CONTINUE
      EPSDMU(I)=(2.*XI)**XNBAR/R**J*FBAR**2*EMUSDMU(I)*RHORHOE(I)**2
     1*SMRER**2
     1*SQRT(ABS(((F2(I+1)-F2(I-1))/(DELETA(I)+DELETA(I-1)))**2
     1+((G2(I+1)-G2(I-1))/(DELETA(I)+DELETA(I-1)))**2
     1*(WEDS2HE/UEDS2HE)**2))
   34 CONTINUE
      IF(IWLDMP.EQ.1.AND.I.NE.2)GO TO 15
      IF(I.NE.2)GO TO 33                              ─── Removed IF(GEE2.NE.0.)GO TO 40
      FDCFD2=((RHORHOE(1)*VWA)/(PHIR(1)/RERS*(2.*R**J)/((2.*XI)**XNBAR)*
     1F2(2)/DELETA(1)*RURDRUS))**2.
      GO TO 41
   40 FDCFD2=((RHORHOE(1)*VWA)/(PHIR(1)/RERS*(2.*R**J)/((2.*XI)**XNBAR)*
     1SQRT((F2(2)/DELETA(1))**2+(G2(2)/DELETA(1))**2*(WEDS2HE/UEDS2HE)**
     22)*RURDRUS))**2.
     2*UEDS2HE/SQRT(WEDS2HE**2+UEDS2HE**2)
   41 CONTINUE
      CALL FTLUP(FDCFD2,AB,1,NFCFAB,FCFTAB,ABTAB)     ─── Removed IF(GEE2.NE.0.)GO TO 35
   15 CONTINUE
      IF(IWLDMP.EQ.1)GO TO 16
      ADL= AB*SQRT((2.*XI)**XNBAR)/(CAPRS*SQRT(EMUSDMU(1))*RHORHOE(1)
     1*RERS
     1*UEDS2HE*SQRT(R**J)*SQRT(ABS(F2(2))/DELETA(1)))
      GO TO 36
   16 ADL=AB*SQRT((2.*XI)**XNBAR)*SQRT(EMUSDMU(1))/(CAPRS*EMUSDMU(I)
     1*SQRT(RHORHOE(1))*SQRT(RHORHOE(I))*RERS
```

```
   1*UEDS2HE*SQRT(R**J)*SQRT(ABS(F2(2))/DELETA(1)))
     GO TO 36
  35 CONTINUE
     ADL= AB*SQRT((2.*XI)**XNBAR)/(CAPRS*SQRT(EMUSDMU(1))*RHORHOE(1)
   1*RERS
   1*UEDS2HE*SQRT(R**J)
   1*((F2(2)/DELETA(1))**2+(G2(2)/DELETA(1))**2*(WEDS2HE/UEDS2HE)**2)
   1**.25)
  36 CONTINUE
  33 EPSDMU(I)=EPSDMU(I)*(1.-EXP(-YDL (I)/ADL))**2
     IF(EPSDMU(I).LT.0.)EPSDMU(I)=0.
     GO TO 31
  32 EPSDMU(I)=0.0
  31 CONTINUE
     IF(IUSEEMU.EQ.0)EPSDMU(I)=0.
     XMBAR(I)=PHIR(I)*(1.+EPSDMU(I))
     XMCIRC(I)=PHIR(I)*(1./SM+EPSDMU(I)/SNT)       Instead of  XMCIRC(I)=XMBAR(I)
     XMSTAR(I)=PHIR(I)/PR*(1.+EPSDMU(I)*PR/PRT)
     ZW=ZETAW
     IF(ZETWTAB(2).EQ.0.)ZW=0.
     IF( MPWEMU.EQ.1)GO TO 37
     XMPRIM(I)=PHIR(I)/PR*(1.-PR)/(1.-ZW)          Instead of ZETAW
     GO TO 10
  37 XMPRIM(I)=PHIR(I)/PR*(1.-PR)/(1.-ZW)*(1.+EPSDMU(I)*PR/PRT*(1.-P   Instead of ZETAW
   1RT)
   1/(1.-PR))
  10 CONTINUE
     RETURN
     END
```

③ {
③
③

```
          SUBROUTINE COMPUTE(NMAX,TEST,NUMDELE,  DELETA,EPSLONE,CAPG,SMLG,
         1 ICHD,DUM2)
          DIMENSION CAPG(350),SMLG(350),DUM2(350),DELETA(350),ZETWTAB(75)
          COMMON/CCW/CCW
          COMMON/ZETW/ZETWTAB
          COMMON/ZETAW2/ZETAW2
      C
      C     T E S T - F I N D I N G   E D G E
      C
          KMAX=NMAX-10
          DO 10 JJ=KMAX,NUMDELE
          TSTVAL=EPSLONE*DELETA(JJ)
          CKVAL=TEST*(1.0-CAPG(JJ))-SMLG(JJ)
          IVAL=JJ+4
          IF(ABS(CKVAL).LE.ABS(TSTVAL))GO TO 20
       10 CONTINUE
       20 NMAX=IVAL
      C
      C     C O M P U T E   D U M 2 S
      C
          NBACK=-(NMAX-1)
          M2=-2
          DO 30 NF=NBACK,M2
          KF=IABS(NF)
          DUM2(KF)=CAPG(KF)*DUM2(KF+1)+SMLG(KF)
       30 CONTINUE
          IF(ICHD.EQ.2)DUM2(1)=CCW=DUM2(2)
          IF(ZETWTAB(2).EQ.0..AND.ICHD.EQ.3)DUM2(1)=ZETAW2=DUM2(2)
          RETURN
          END
```

③ {

③ {

# REFERENCES

1. Wieghardt, K.: On the Blowing of Warm Air for De-Icing-Devices. Rep. Transl. No. 315, Brit. M.A.P. Völkenrode, Nov. 1946.

2. Papell, S. Stephen; and Trout, Arthur M.: Experimental Investigation of Air Film Cooling Applied to an Adiabatic Wall by Means of an Axially Discharging Slot. NASA TN D-9, 1959.

3. Dunavant, James C.; and Everhart, Philip E.: Exploratory Heat-Transfer Measurements at Mach 10 on a 7.5° Total-Angle Cone Downstream of a Region of Air and Helium Transpiration Cooling. NASA TN D-5554, December 1969.

4. Newman, B. G.: The Prediction of Turbulent Jets and Wall Jets. Can. Aeronaut. Space J., vol. 15, no. 8, Oct. 1969, pp. 288-305.

5. Seban, R. A.; and Back, L. H.: Velocity and Temperature Profiles in a Wall Jet. Int. J. Heat Mass Transfer, vol. 3, no. 4, Dec. 1961, pp. 255-265.

6. Chin, J. H.; Skirvin, S. C.; Hayes, L. E.; and Silver, A. H.: Adiabatic Wall Temperature Downstream of a Single, Tangential Injection Slot. Pap. No. 58-A-107, Amer. Soc. Mech. Eng., 1958.

7. Seban, R. A.: Heat Transfer and Effectiveness for a Turbulent Boundary Layer With Tangential Fluid Injection. Trans. ASME, Ser. C: J. Heat Transfer, vol. 82, no. 4, Nov. 1960, pp. 303-312.

8. Hartnett, J. P.; Birkebak, R. C.; Eckert, E. R. G.: Velocity Distributions, Temperature Distributions, Effectiveness and Heat Transfer for Air Injected Through a Tangential Slot Into a Turbulent Boundary Layer. Trans. ASME, Ser. C: J. Heat Transfer, vol. 83, no. 3, Aug. 1961, pp. 293-306.

9. Seban, R. A.; and Back, L. H.: Velocity and Temperature Profiles in Turbulent Boundary Layers With Tangential Injection. Trans. ASME, Ser. C: J. Heat Transfer, vol. 84, no. 1, Feb. 1962, pp. 45-54.

10. Eckert, E. R. G.; and Birkebak, R. C.: The Effects of Slot Geometry on Film Cooling. Heat Transfer, Thermodynamics, and Eduction, Harold A. Johnson, ed., McGraw-Hill Book Co., Inc., c.1964, pp. 150-163.

11. Whitelaw, James H.: An Experimental Investigation of the Two-Dimensional Wall Jet. C.P. No. 942, Brit. A.R.C., 1967.

12. Sivasegaram, S.; and Whitelaw, J. H.: Film Cooling Slots: The Importance of Lip Thickness and Injection Angle. J. Mech. Eng. Sci., vol. 11, no. 1, 1969, pp. 22-27.

13. Burns, W. K.; and Stollery, J. L.: The Influence of Foreign Gas Injection and Slot Geometry on Film Cooling Effectiveness. Int. J. Heat Mass Transfer, vol. 12, no. 8, Aug. 1969, pp. 935-951.

14. Pai, B. R.; and Whitelaw, J. H.: The Influence of Density Gradients on the Effectiveness of Film Cooling. C.P. No. 1013, Brit. A.R.C., 1968.

15. Seban, R. A.; and Back, L. H.: Effectiveness and Heat Transfer for a Turbulent Boundary Layer With Tangential Injection and Variable Free-Stream Velocity. Trans. ASME, Ser. C: J. Heat Transfer, vol. 84, no. 3, Aug. 1962, pp. 235-244.

16. Carlson, L. W.; and Talmor, E.: Gaseous Film Cooling at Various Degrees of Hot-Gas Acceleration and Turbulence Levels. Int. J. Heat Mass Transfer, vol. 11, no. 11, Nov. 1968, pp. 1695-1713.

17. Chin, J. H.; Skirvin, S. C.; Hayes, L. E.; and Burggraf, F.: Film Cooling With Multiple Slots and Louvers. Trans. ASME, Ser. C: J. Heat Transfer, vol. 83, no. 3, Aug. 1961, pp. 281-292.
    Pt. 1 — Multiple Continuous Slots.
    Pt. 2 — Multiple Rows of Discrete Louvers.

18. Sellers, John P., Jr.: Gaseous Film Cooling With Multiple Injection Stations. AIAA J., vol. 1, no. 9, Sept. 1963, pp. 2154-2156.

19. Repukhov, V. M.; and Bogachuk-Kozachuk, K. A.: Film Cooling Effectiveness of a Flat Surface for a Turbulent Boundary Layer Behind Tangential Slots. Heat Transfer — Soviet Res., vol. 1, no. 3, May 1969, pp. 163-168.

20. Laganelli, A. L.: A Comparison Between Film Cooling and Transpiration Cooling Systems in High Speed Flow. AIAA Pap. No. 70-153, Jan. 1970.

21. Peterson, John B., Jr.; McRee, Donald I.; Adcock, Jerry B.; and Braslow, Albert L.: Further Investigation of Effect of Air Injection Through Slots and Porous Surfaces on Flat-Plate Turbulent Skin Friction at Mach 3. NASA TN D-3311, 1966.

22. Parthasarathy, K.; and Zakkay, V.: An Experimental Investigation of Turbulent Slot Injection at Mach 6. AIAA J., vol. 8, no. 7, July 1970, pp. 1302-1307.

23. Parthasarathy, K.; and Zakkay, V.: Turbulent Slot Injection Studies at Mach 6. ARL 69-0066, U.S. Air Force, Apr. 1969. (Available from DDC as AD 692 503.)

24. Zakkay, V.; Sakell, L.; and Parthasarathy, K.: An Experimental Investigation of Supersonic Slot Cooling. Proceedings of the 1970 Heat Transfer and Fluid Mechanics Institute, Turgut Sarpkaya, ed., Stanford Univ. Press, 1970, pp. 88-103.

25. Goldstein, R. J.; Eckert, E. R. G.; Tsou, F. K.; and Haji-Sheikh, A.: Film Cooling With Air and Helium Injection Through a Rearward-Facing Slot Into a Supersonic Air Flow. AIAA J., vol. 4, no. 6, June 1966, pp. 981-985.

26. Schetz, Joseph A.; and Gilreath, Harold E.: Tangential Slot Injection in Supersonic Flow. AIAA J., vol. 5, no. 12, Dec. 1967, pp. 2149-2154.

27. Schetz, Joseph A.; Gilreath, Harold E.; and Lubard, Stephen C.: Fuel Injection and Mixing in a Supersonic Stream. Twelfth Symposium (International) on Combustion, Combustion Inst., 1969, pp. 1141-1149.

28. Schetz, Joseph A.; Gilreath, Harold E.; Waltrup, Paul J.; and Lewis, David P.: Research on Slot Injection Into a Supersonic Air Stream. AFAPL-TR-68-97, U.S. Air Force, Sept. 1968. (Available from DDC as AD 839 872.)

29. Cary, Aubrey M., Jr.; and Hefner, Jerry N.: Film Cooling Effectiveness in Hypersonic Turbulent Flow. AIAA J., vol. 8, no. 11, Nov. 1970, pp. 2090-2091.

30. Eckert, Ernst R. G.: Survey on Heat Transfer at High Speeds. WADC Tech. Rep. 54-70, U.S. Air Force, Apr. 1954.

31. Conti, Raul J.: Heat-Transfer Measurements at a Mach Number of 2 in the Turbulent Boundary Layer on a Flat Plate Having a Stepwise Temperature Distribution. NASA TN D-159, 1959.

32. Klein, John; and Tribus, Myron: Forced Convection From Nonisothermal Surfaces. Project M992-B (Contract AF 18(600)-51, E. O. No. 462-BR-1), Eng. Res. Inst., Univ. of Michigan, Aug. 1952.

33. Gosman, A. D.; Pun, W. M.; Runchal, A. K.; Spalding, D. B.; and Wolfshtein, M.: Heat and Mass Transfer in Recirculating Flows. Academic Press, Inc., 1969.

34. Pletcher, Richard H.: On a Solution for Turbulent Boundary Layer Flows With Heat Transfer, Pressure Gradients, and Wall Blowing or Suction. Heat Transfer 1970, Vol. II, Ulrich Grigull and Erich Hahne, eds., Elsevier Pub. Co. (Amsterdam), 1970, pp. FC 2.9.1-FC 2.9.12.

35. Cebeci, Tuncer; Smith, A. M. O.; and Mosinskis, G.: Calculation of Compressible Adiabatic Turbulent Boundary Layers. AIAA Pap. No. 69-687, June 1969.

36. Bushnell, Dennis M.; and Beckwith, Ivan E.: Calculation of Nonequilibrium Hypersonic Turbulent Boundary Layers and Comparisons With Experimental Data. AIAA J., vol. 8, no. 8, Aug. 1970, pp. 1462-1469.

37. Patankar, S. V.; and Spalding, D. B.: Heat and Mass Transfer in Boundary Layers. Morgan-Grampian (London), 1967.

38. Kacker, S. C.; Pai, B. R.; and Whitelaw, J. H.:   The Prediction of Wall Jet Flows With Particular Reference to Film Cooling.   Vol. 2 of Progress in Heat and Mass Transfer.   Thomas F. Irvine, Jr., Warren E. Ibele, James P. Hartnett, and Richard J. Goldstein, eds., Pergamon Press, Inc., 1969, pp. 163-186.

39. Kacker, S. C.; and Whitelaw, J. H.:   Some Properties of the Two-Dimensional, Turbulent Wall Jet in a Moving Stream.   Trans. ASME, Ser. E:   J. Appl. Mech., vol. 35, no. 4, Dec. 1968, pp. 641-651.

40. Beckwith, Ivan E.:   Recent Advances in Research on Compressible Turbulent Boundary Layers.   NASA SP-228, 1969, pp. 355-416.

41. Hixon, Barbara A.; Beckwith, Ivan E.; and Bushnell, Dennis M.:   Computer Program for Compressible Laminar or Turbulent Nonsimilar Boundary Layers.   NASA TM X-2140, 1971.

42. Herring, H. James; and Mellor, George L.:   A Method of Calculating Compressible Turbulent Boundary Layers.   NASA CR-1144, 1968.

43. Eskinazi, S.; and Erian, F. F.:   Energy Reversal in Turbulent Flows.   Phys. Fluids, vol. 12, no. 10, Oct. 1969, pp. 1988-1998.

44. Peters, C. E.; Chriss, D. E.; and Paulk, R. A.:   Turbulent Transport Properties in Subsonic Coaxial Free Mixing Systems.   AIAA Pap. No. 69-681, June 1969.

45. Harvey, William D.; Bushnell, Dennis M.; and Beckwith, Ivan E.:   Fluctuating Properties of Turbulent Boundary Layers for Mach Numbers up to 9.   NASA TN D-5496, 1969.

46. Kiser, K. M.:   Material and Momentum Transport in Axisymmetric Turbulent Jets of Water.   Amer. Inst. Chem. Eng. J., vol. 9, no. 3, May 1963, pp. 386-390.

47. Hinze, J. O.:   Turbulence.   McGraw-Hill Book Co., Inc., 1959.

48. Liepmann, Hans Wolfgang; and Laufer, John:   Investigations of Free Turbulent Mixing. NACA TN 1257, 1947.

49. Bradbury, L. J. S.:   The Structure of a Self-Preserving Turbulent Plane Jet.   J. Fluid Mech., vol. 23, pt. 1, Sept. 1965, pp. 31-64.

50. Schlichting, Hermann (J. Kestin, transl.):   Boundary-Layer Theory.   Sixth ed., McGraw-Hill Book Co., 1968.

51. Williamson, John W.:   An Extension of Prandtl's Mixing Length Theory.   69-FE-48, Amer. Soc. Mech. Eng., 1969.

52. Garringer, Darwin J.; and Saltzman, Edwin J.:   Flight Demonstration of a Skin-Friction Gage to a Local Mach Number of 4.9.   NASA TN D-3830, 1967.

53. Haering, George William: Boundary Layer Separation Control and Wall Temperature Control by Tangential Fluid-Injection. Ph. D. Diss., Ohio State Univ., 1968.
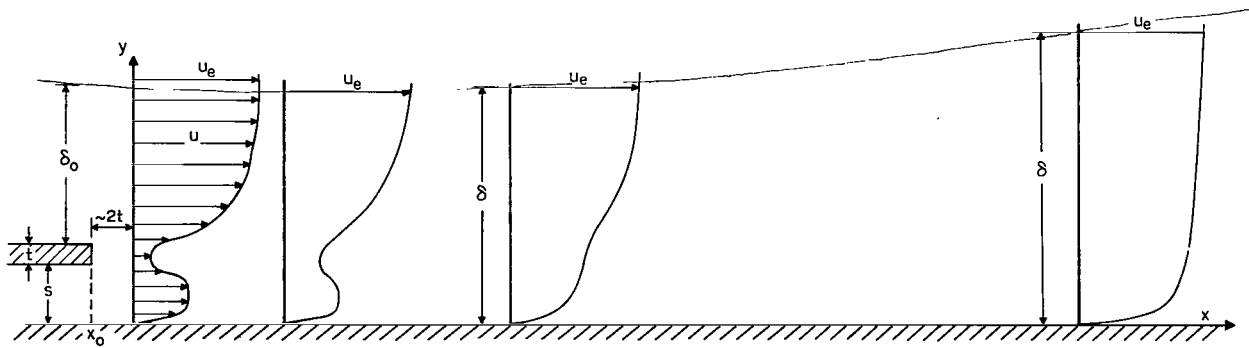
(a) Velocity profiles.
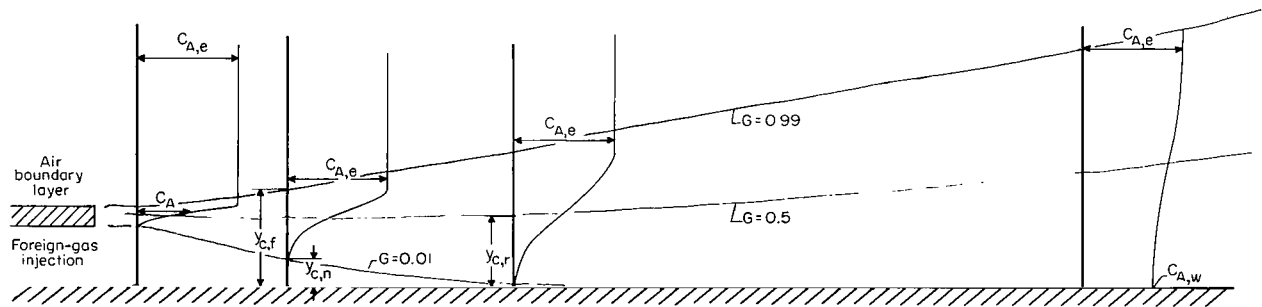


(b) Concentration of air with foreign-gas injection.
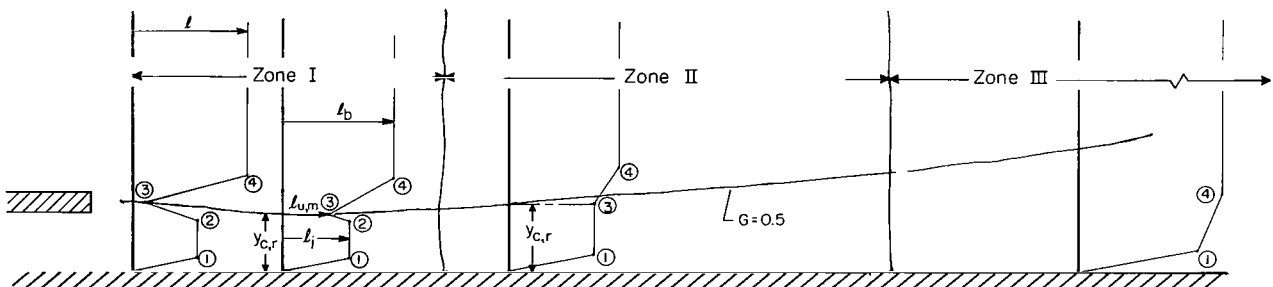


(c) Mixing-length distribution.

Figure 1.- Schematic sketch of velocity, concentration, and mixing-length profiles for hypothetical slot-injection flow.
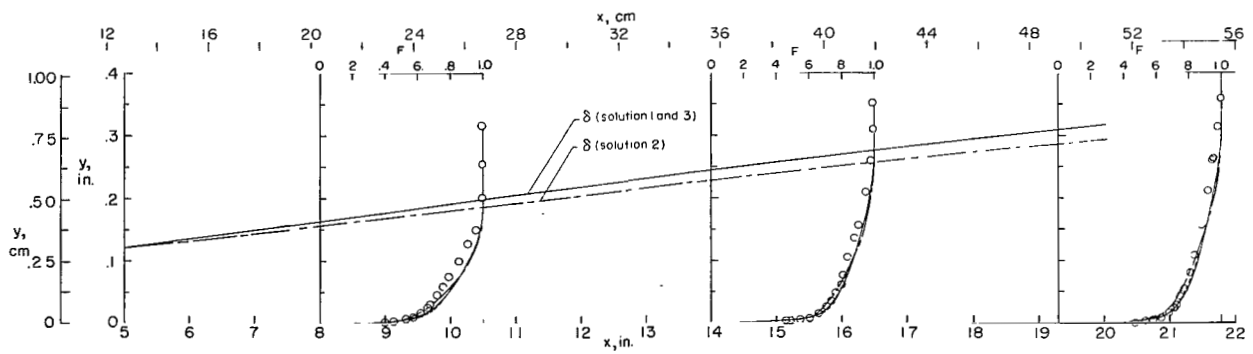
(a) Velocity profiles.   x < 11.7 cm  (4.6 in.).



(b)   G   profiles and lines of constant   G.   x < 11.7 cm  (4.6 in.).



(c) Mixing-length distributions.   x < 11.7 cm  (4.6 in.).
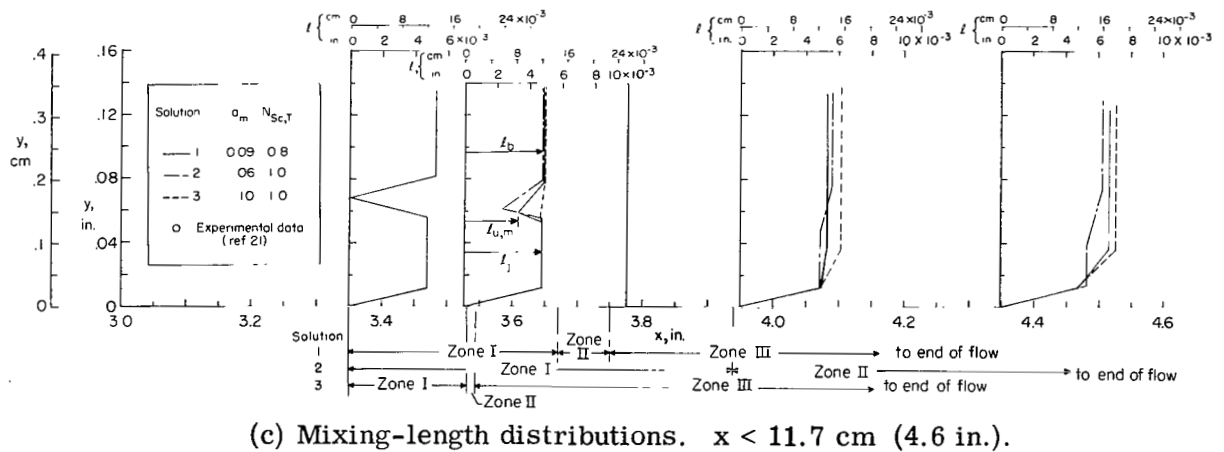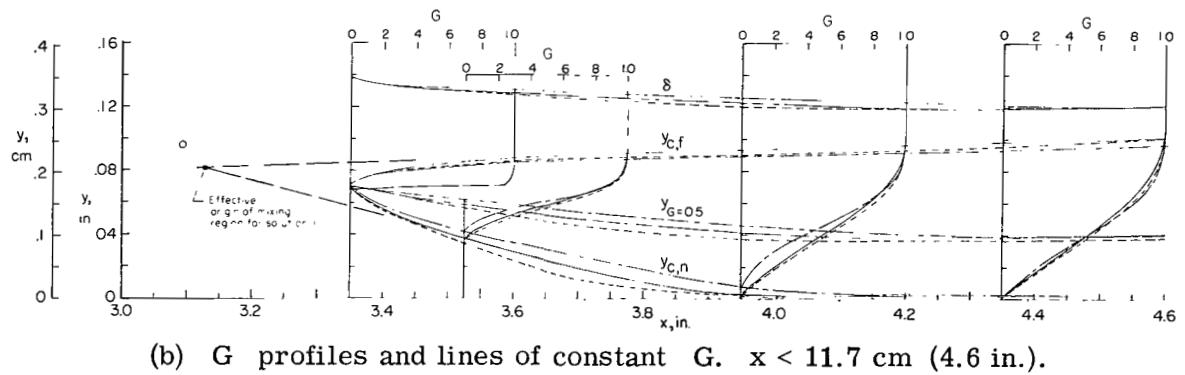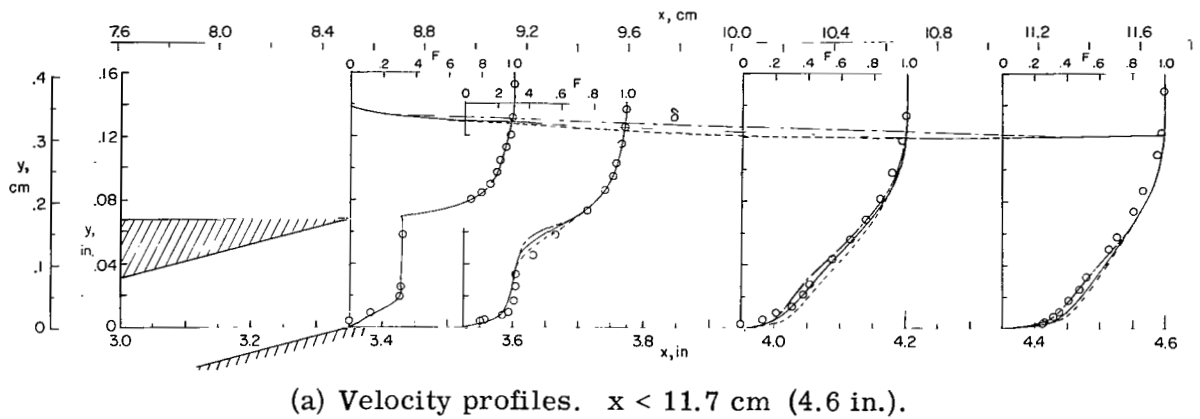
Figure 2.- Theoretical predictions for velocity and concentration profiles and mixing-
length distributions for   s = 1.73 mm (0.068 in.)   rearward inclined step slot configu-
ration of reference 21.   Experimental data for velocity profiles are shown for compari-
son.   $a_j = 0.14$   used for all solutions; $y_{c,f}$   and   $y_{c,n}$   evaluated at   G = 0.99   and
G = 0.01, respectively;   t = 0.025 mm (0.001 in.)   used in calculations.

(d) Velocity profiles. x > 12.7 cm (5.0 in.).
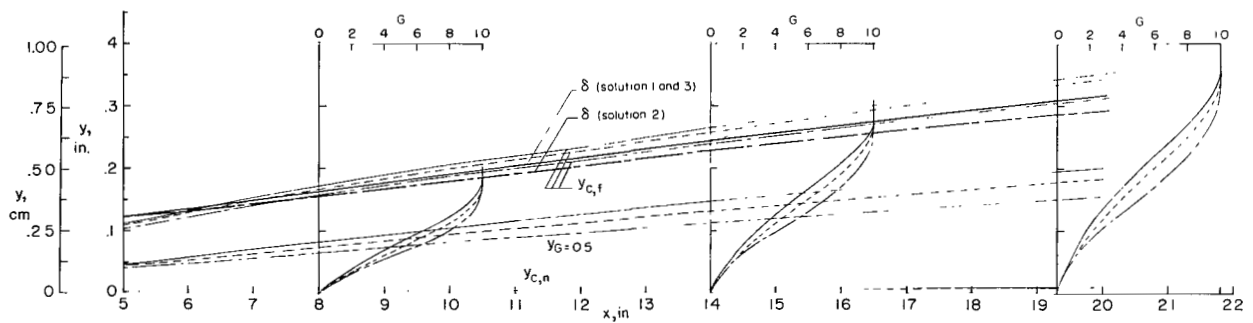


(e) G profiles and lines of constant G. x > 12.7 cm (5.0 in.).



| Solution | $\sigma_m$ | $N_{Sc,T}$ |
|----------|-----------|-----------|
| ——— 1   | 009       | 08        |
| —·— 2    | 06        | 10        |
| ——— 3    | 10        | 10        |
| O Experimental data (ref 21) | | |
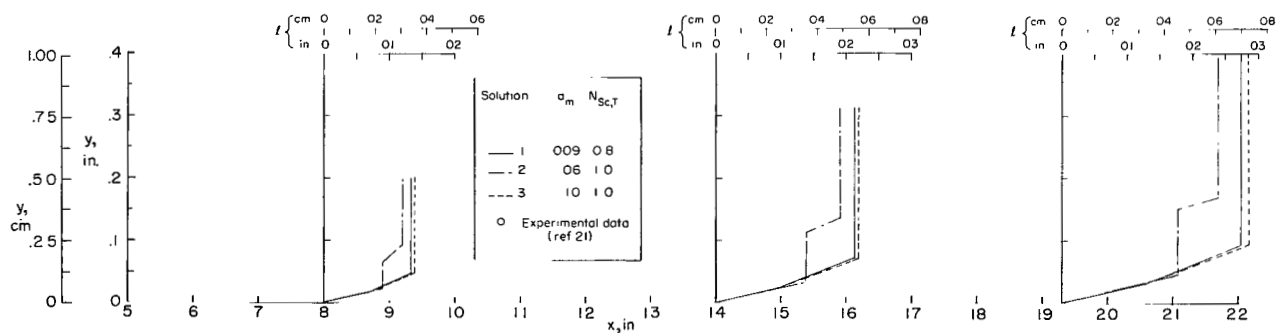
(f) Mixing-length distributions. x > 12.7 cm (5.0 in.).

Figure 2.- Concluded.
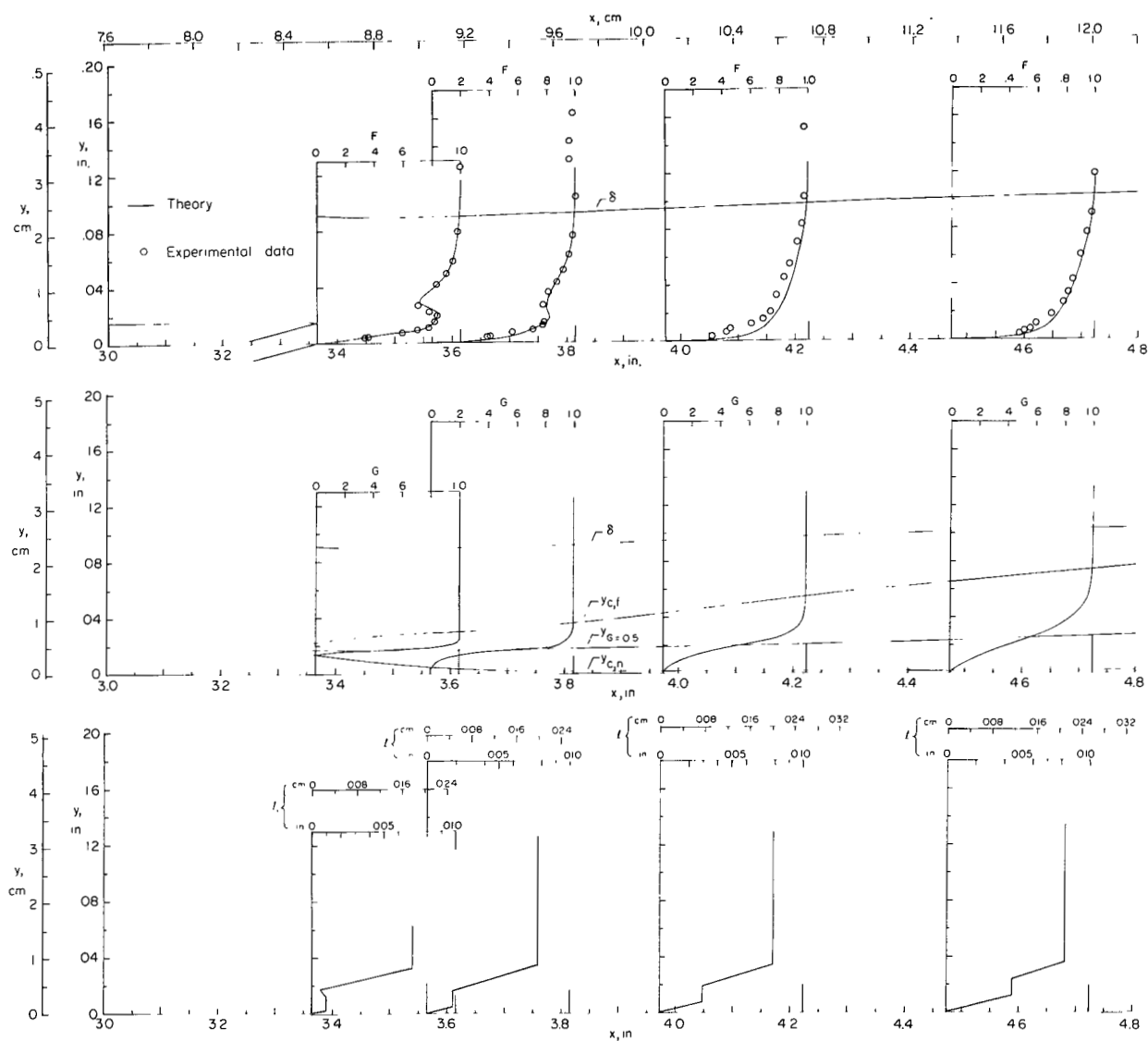
(a)  x < 12.2 cm  (4.8 in.).

Figure 3.- Comparison of predicted and experimental velocity profiles from data
of reference 21 for rearward inclined step slot with  s = 0.038 cm  (0.015 in.).
$a_j = 0.14$;  $a_m = 0.09$;  $N_{Sc,T} = 0.8$.

66
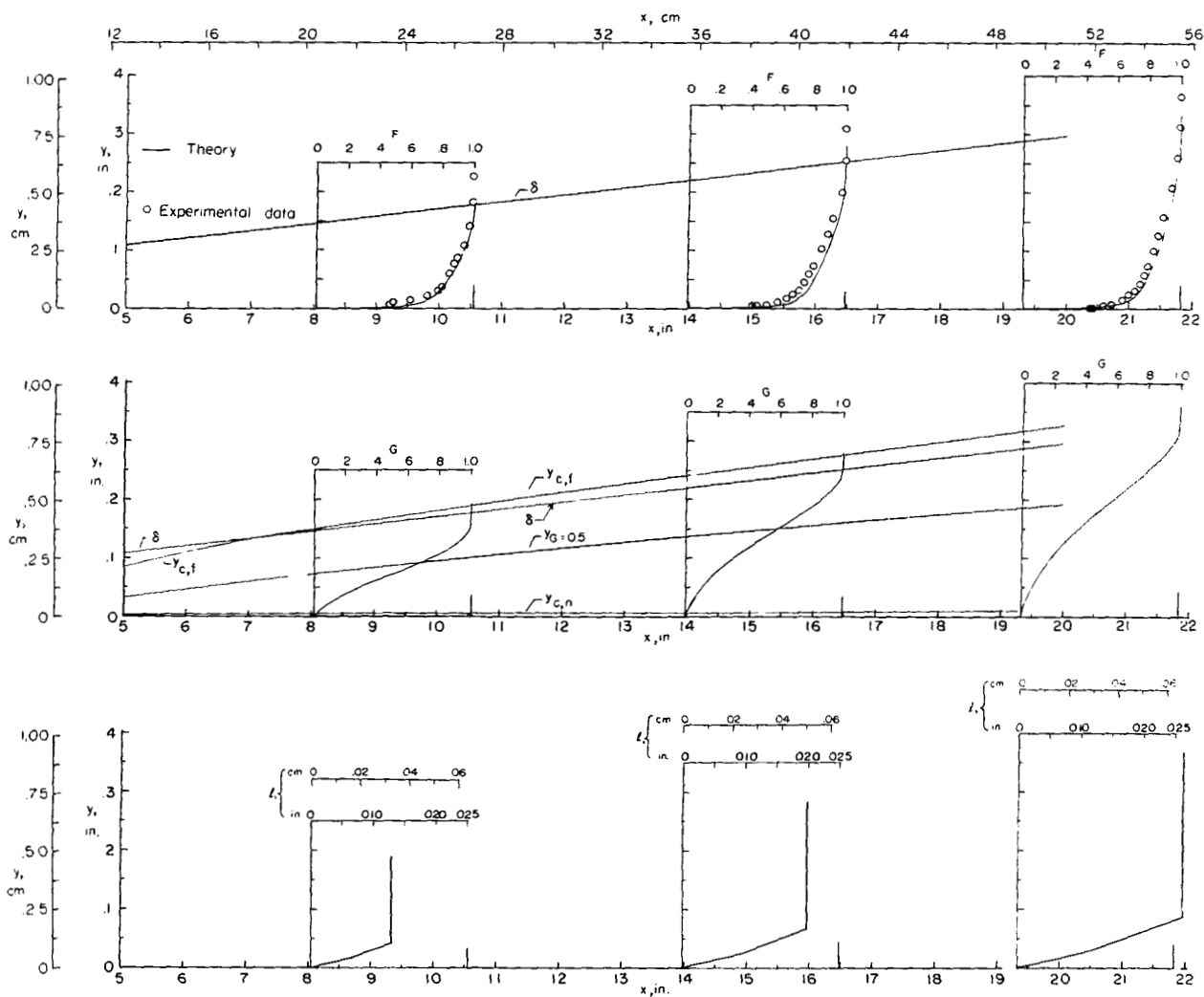
(b)  x > 12.7 cm (5.0 in.).

Figure 3.- Concluded.
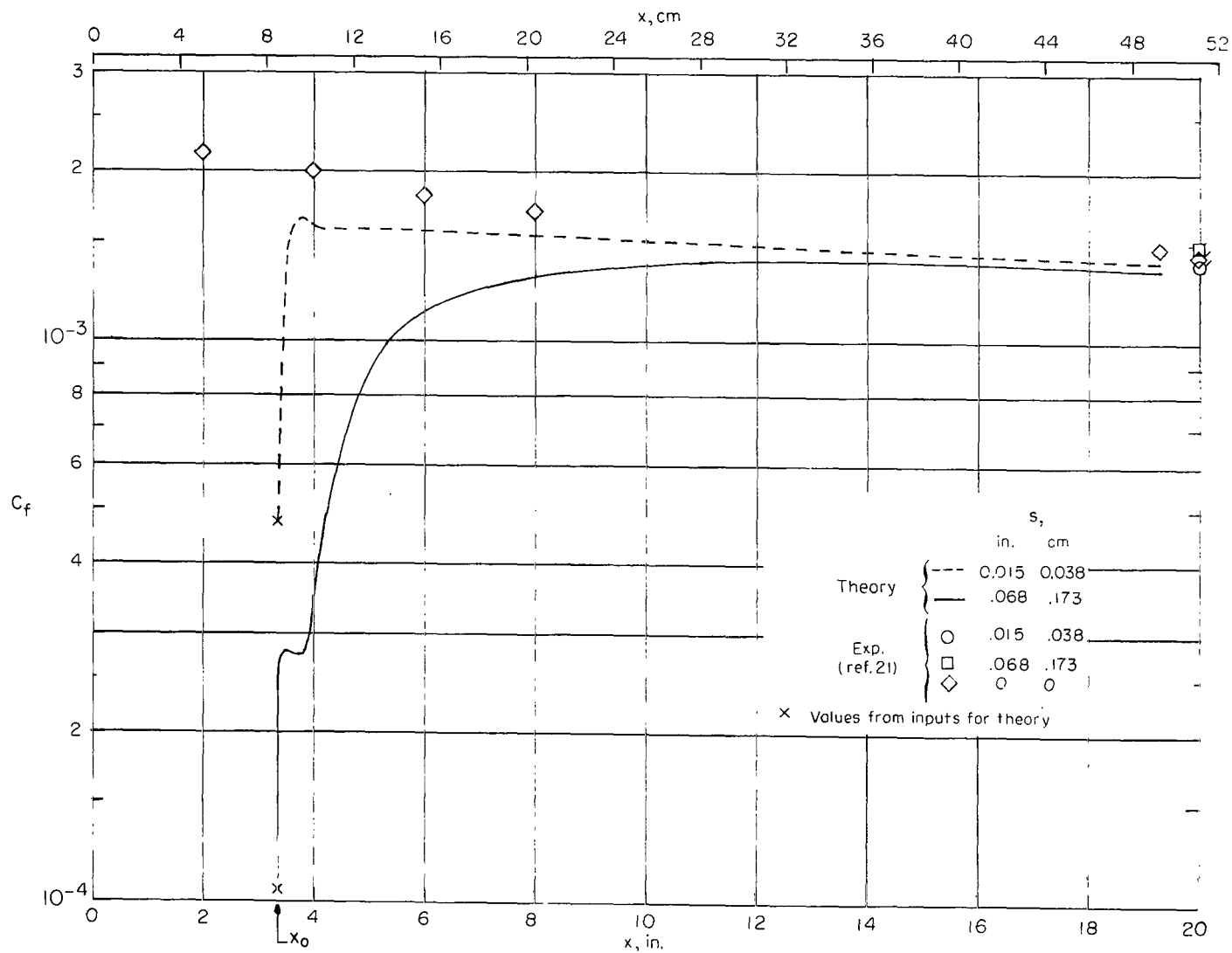
Figure 4.- Calculated distribution of skin friction for $a_j = 0.14$, $a_m = 0.09$, and $N_{Sc,T} = 0.8$ and comparison with experimental data from reference 21. Flagged symbols at $x = 50.8$ cm (20 in.) are skin-friction balance data and unflagged symbols are from measurements of $\theta$ on solid flat plate without a slot.
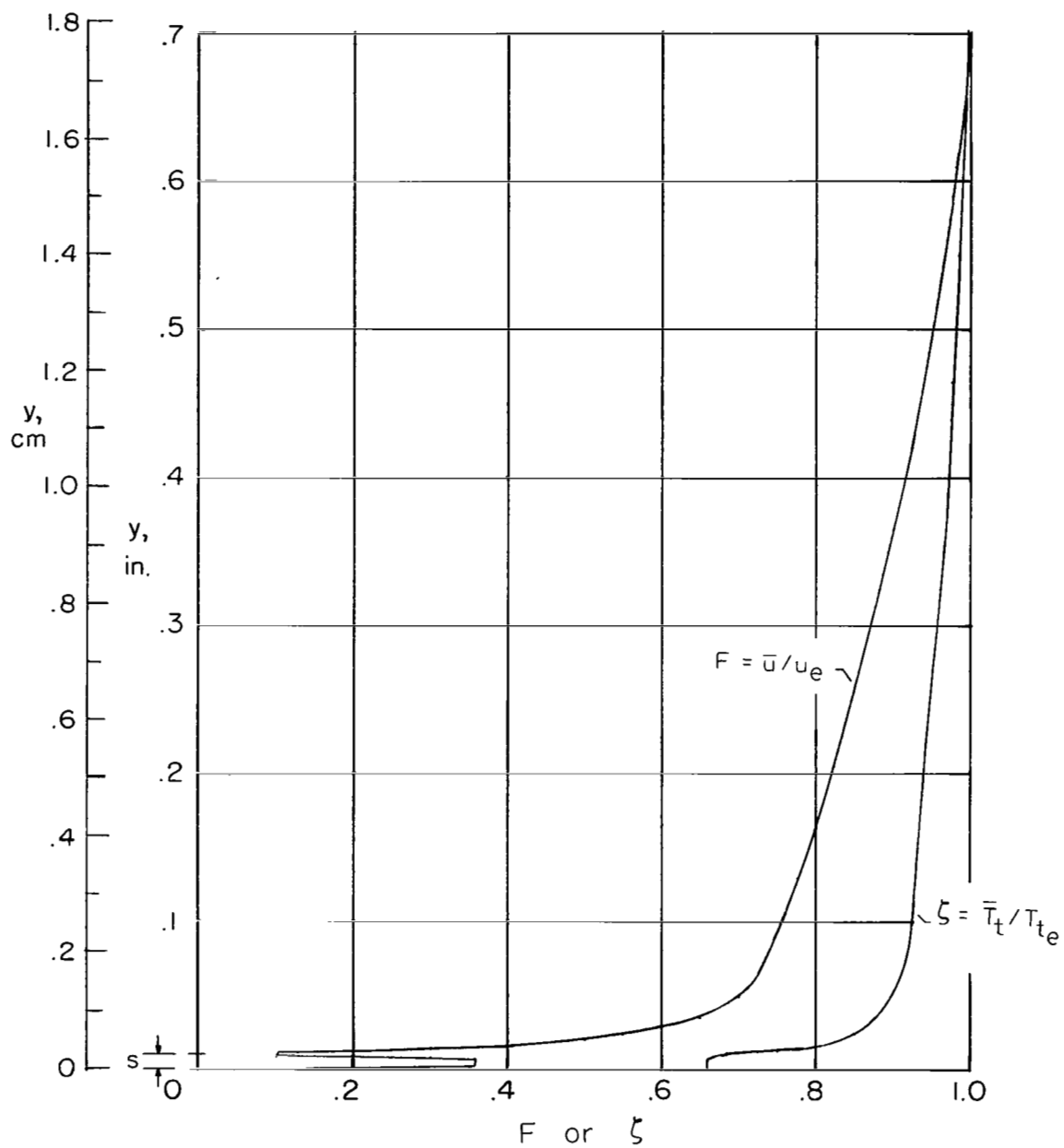
Figure 5.- Initial profiles at $x_O$ based on data from reference 23.
$M_e = 6$; $T_{t,e} \approx 444^O$ K $(800^O$ R); $T_{t,j} \approx 294^O$ K $(530^O$ R);
$s = 0.25$ mm $(0.01$ in.); $\lambda = 0.068$.
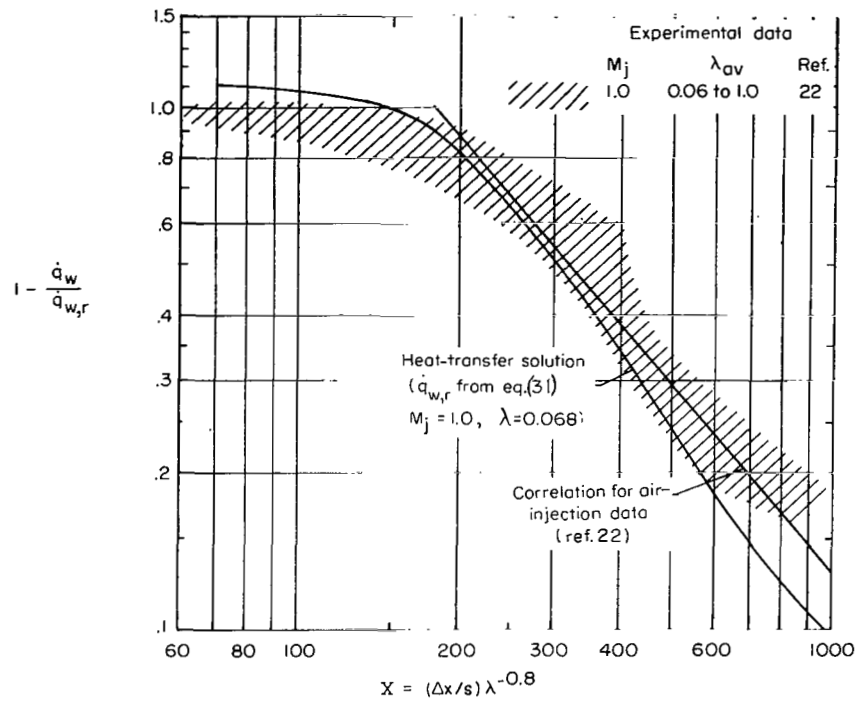
Figure 6.- Comparison of computed heat-transfer distribution with experimental data of reference 22.
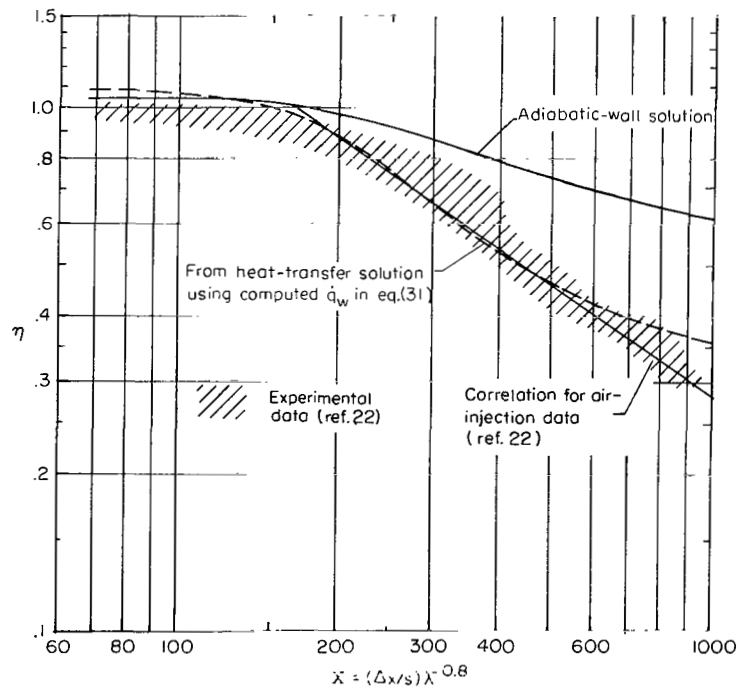


Figure 7.- Comparisons of calculated values of effectiveness with experimental data from reference 22.

70
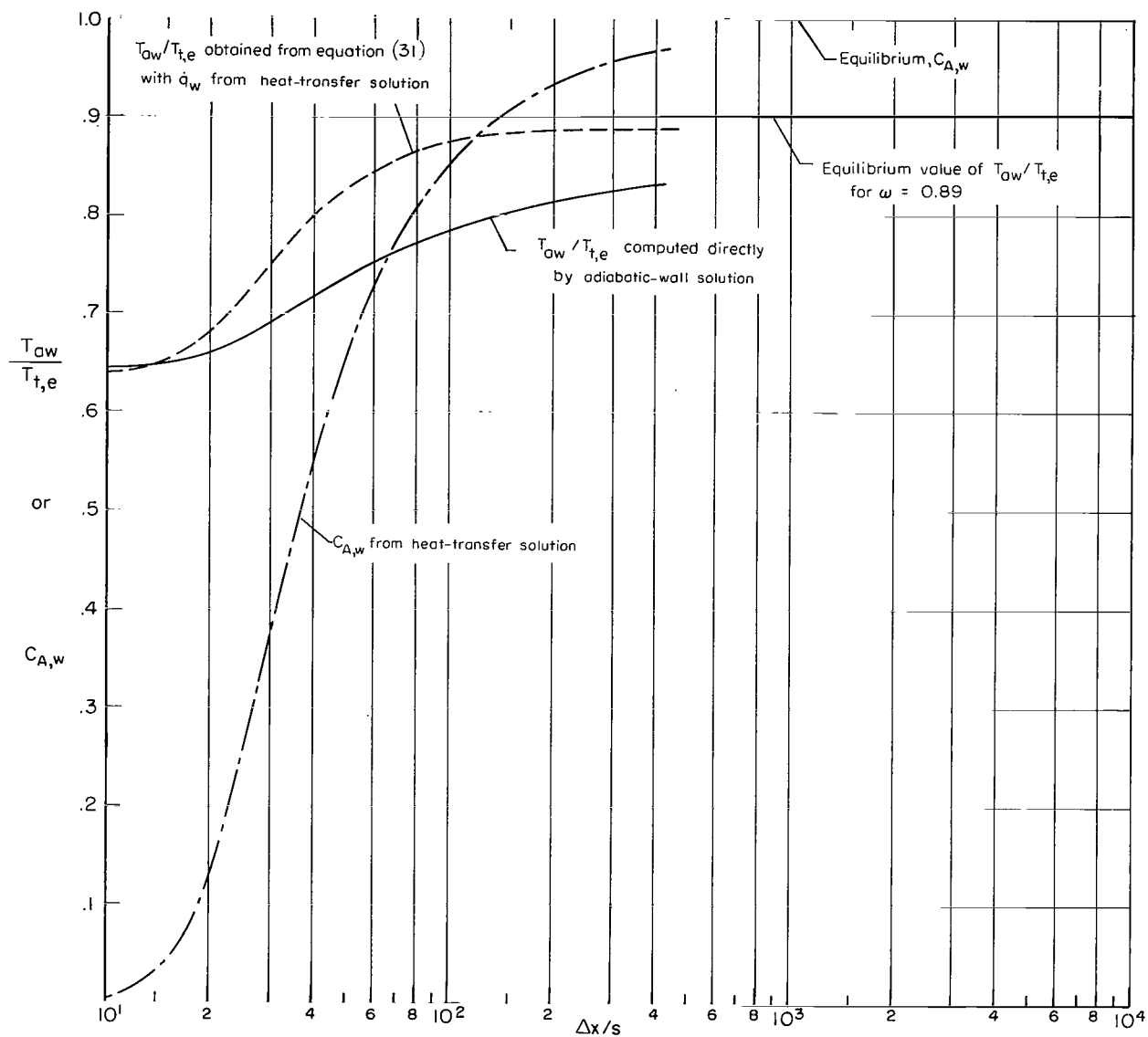
Figure 8.- Calculated distributions of wall-recovery temperature and trace mass concentration at the wall for test conditions of reference 22.
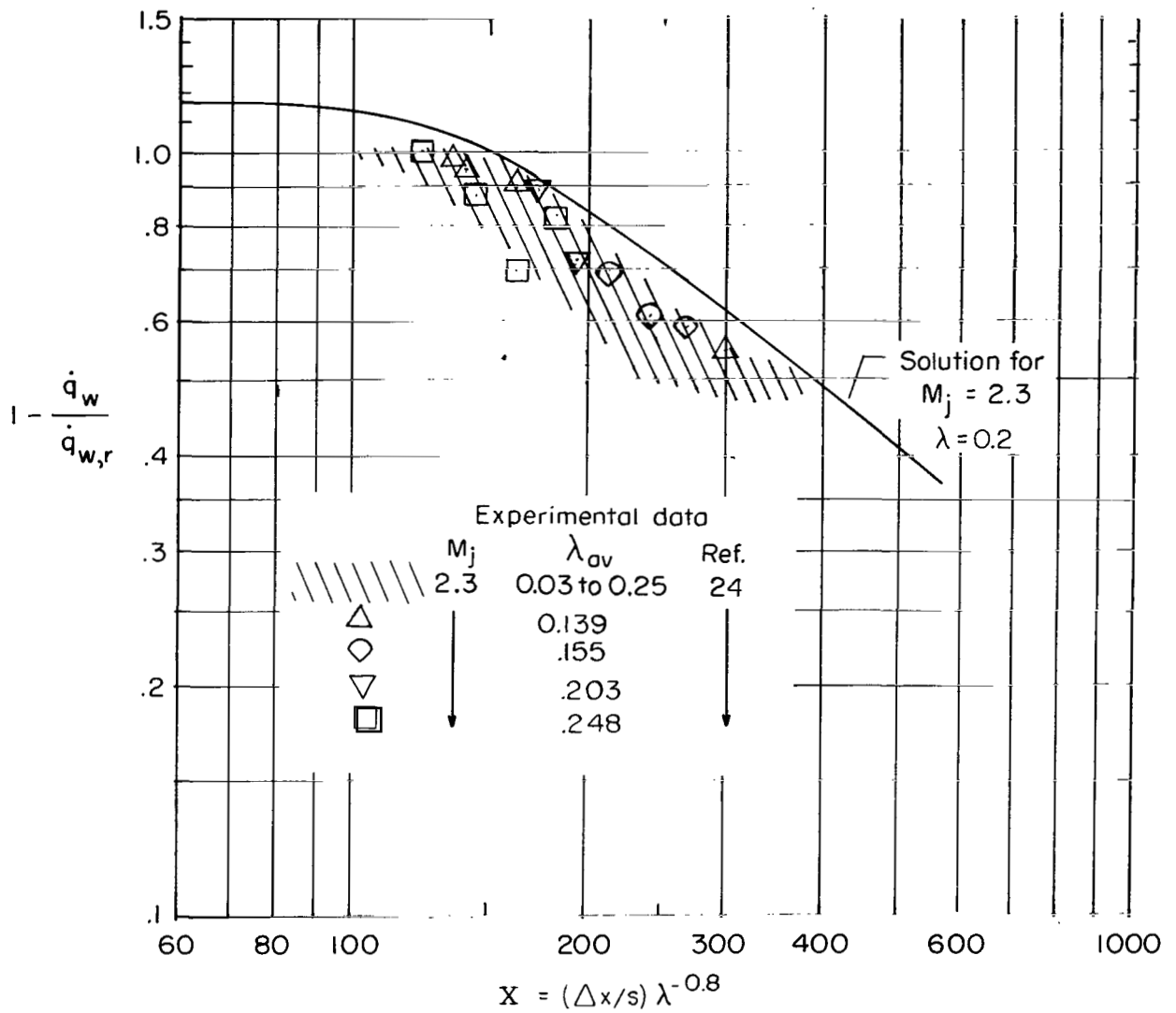
Figure 9.- Comparison of computed heat-transfer distribution with experimental data of reference 24.
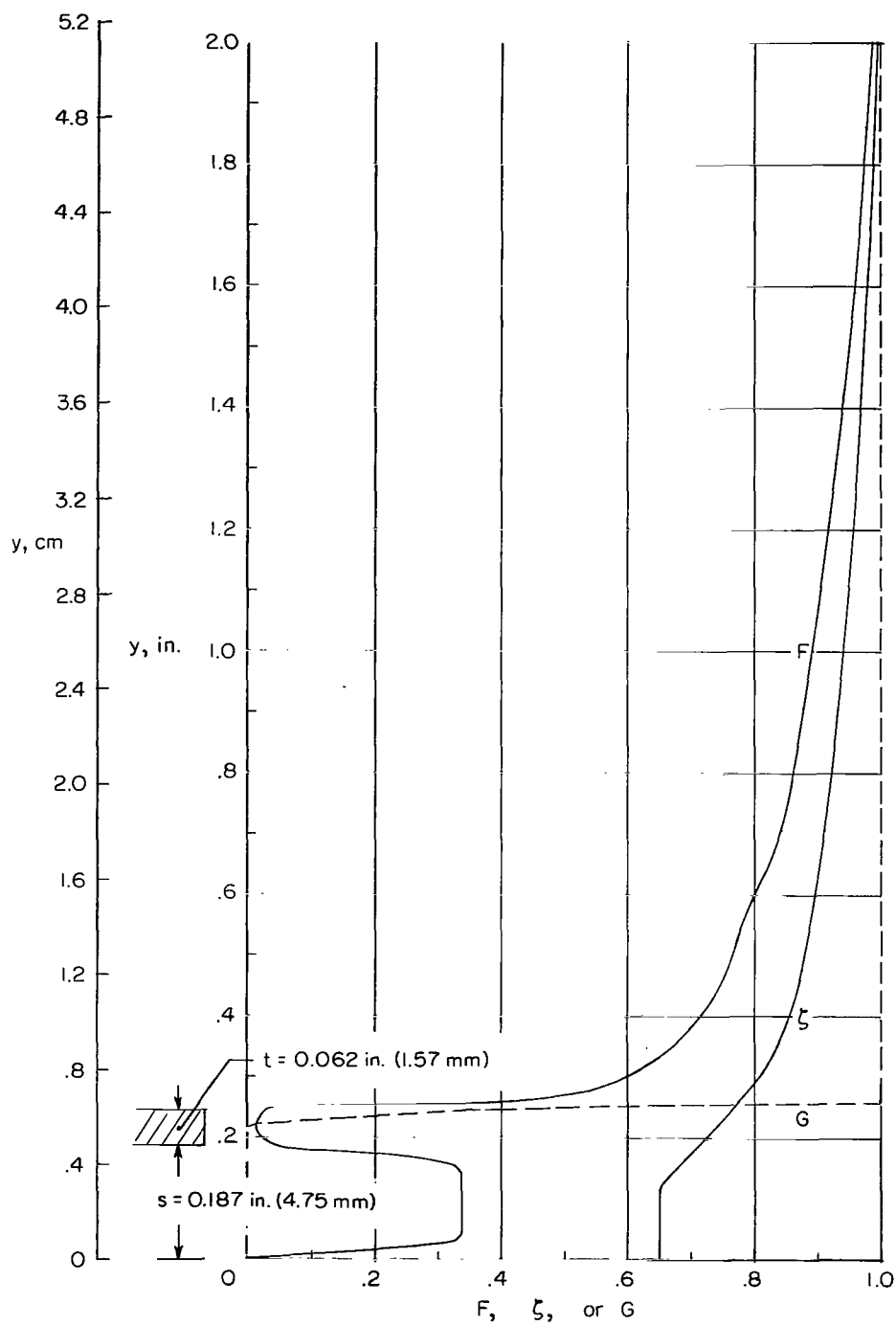
Figure 10.- Initial profiles used in solution for conditions of reference 29.   $M_e = 6.0$.
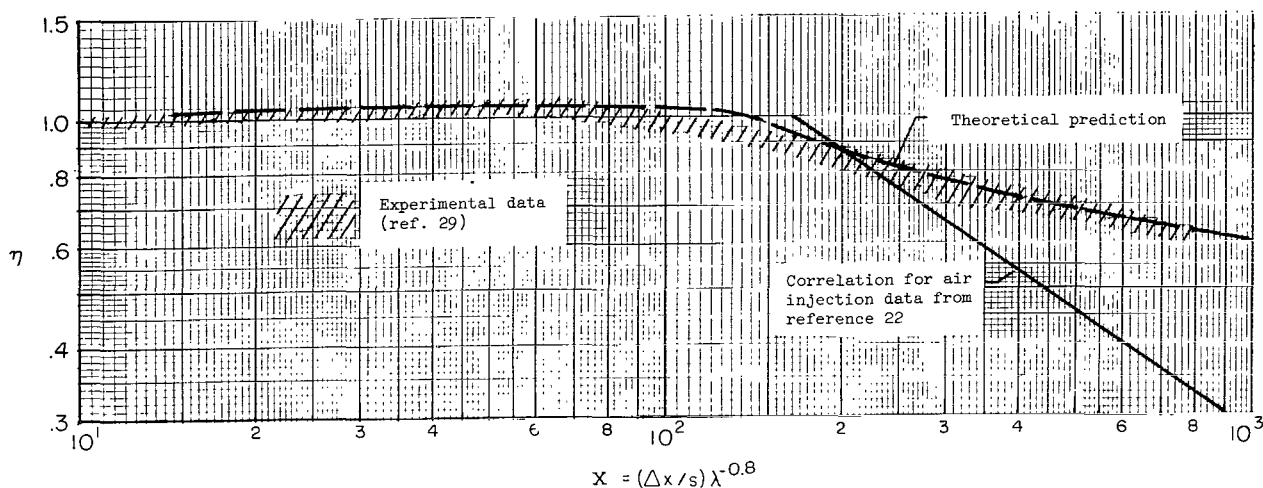
Figure 11.- Comparison of predicted effectiveness with experimental data for $M_e = 6.0$ and $\lambda = 0.06$ to $1.6$ (ref. 29) based on direct measurements of recovery temperature for $s = 0.15$ to $1.12$ cm $(0.06$ to $0.44$ in.$)$. Values of input parameters in theory were $\lambda = 0.065$, $M_e = 6.0$, $a_j = 0.14$, $s = 4.78$ mm $(0.188$ in.$)$, $a_m = 0.09$, and $N_{Sc,T} = 0.8$.
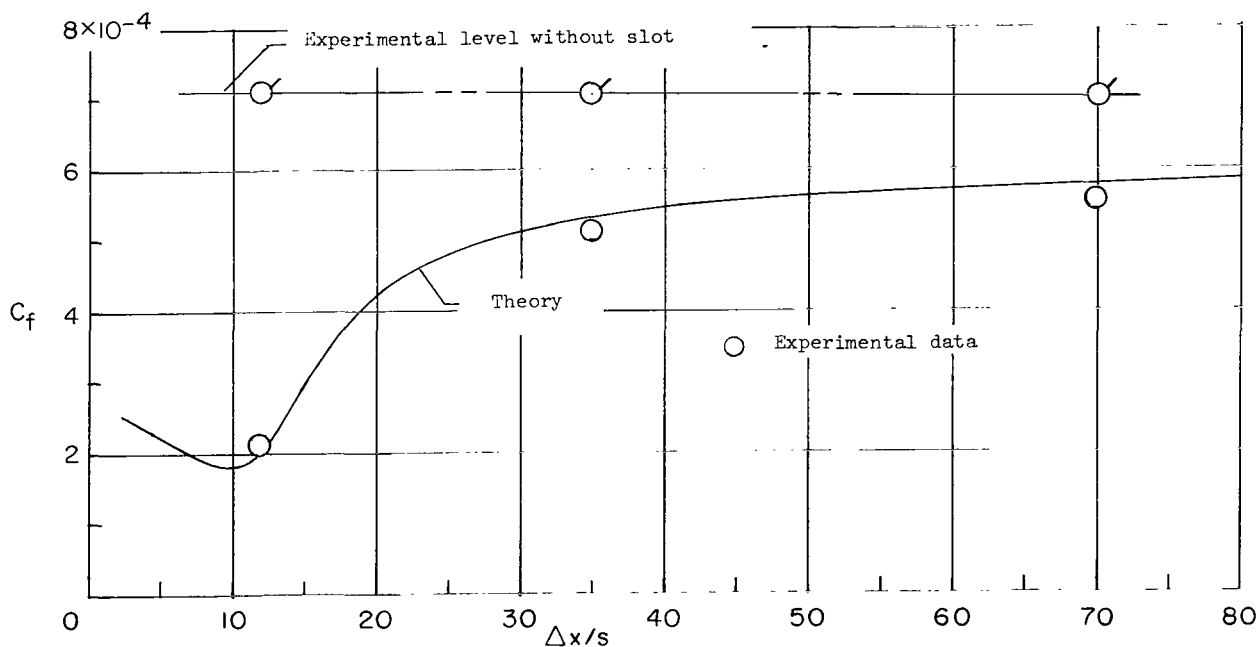


Figure 12.- Comparison of $C_f$ prediction from finite-difference solution with experimental values obtained by Cary from skin-friction balance. Flagged symbols are measured values without slot. $s = 4.78$ mm $(0.188$ in.$)$; $t = 1.57$ mm $(0.062$ in.$)$; $\lambda = 0.065$; $\delta_0 = 50.8$ mm $(2.0$ in.$)$; $T_{t,j}/T_{t,e} = 0.63$.

*"The aeronautical and space activities of the United States shall be conducted so as to contribute . . . to the expansion of human knowledge of phenomena in the atmosphere and space. The Administration shall provide for the widest practicable and appropriate dissemination of information concerning its activities and the results thereof."*

— NATIONAL AERONAUTICS AND SPACE ACT OF 1958

# NASA SCIENTIFIC AND TECHNICAL PUBLICATIONS

**TECHNICAL REPORTS:** Scientific and technical information considered important, complete, and a lasting contribution to existing knowledge.

**TECHNICAL NOTES:** Information less broad in scope but nevertheless of importance as a contribution to existing knowledge.

**TECHNICAL MEMORANDUMS:** Information receiving limited distribution because of preliminary data, security classification, or other reasons.

**CONTRACTOR REPORTS:** Scientific and technical information generated under a NASA contract or grant and considered an important contribution to existing knowledge.

**TECHNICAL TRANSLATIONS:** Information published in a foreign language considered to merit NASA distribution in English.

**SPECIAL PUBLICATIONS:** Information derived from or of value to NASA activities. Publications include conference proceedings, monographs, data compilations, handbooks, sourcebooks, and special bibliographies.

**TECHNOLOGY UTILIZATION PUBLICATIONS:** Information on technology used by NASA that may be of particular interest in commercial and other non-aerospace applications. Publications include Tech Briefs, Technology Utilization Reports and Technology Surveys.

*Details on the availability of these publications may be obtained from:*

## SCIENTIFIC AND TECHNICAL INFORMATION OFFICE

# NATIONAL AERONAUTICS AND SPACE ADMINISTRATION
### Washington, D.C. 20546